

# Link representation of the entanglement entropies for all bipartitions

Sudipto Singha Roy,<sup>1</sup> Silvia N. Santalla,<sup>2</sup> Germán Sierra,<sup>1</sup> and Javier Rodríguez-Laguna<sup>3</sup>

<sup>1</sup>*Instituto de Física Teórica UAM/CSIC, Universidad Autónoma de Madrid, Cantoblanco, Madrid, Spain*

<sup>2</sup>*Dep. de Física and Grupo Interdisciplinar de Sistemas Complejos (GISC), Universidad Carlos III de Madrid, Spain*

<sup>3</sup>*Dep. de Física Fundamental, UNED, Madrid, Spain*

(Dated: March 17, 2021)

We have recently shown that the entanglement entropy of any bipartition of a quantum state can be approximated as the sum of certain link strengths connecting internal and external sites. The representation is useful to unveil the geometry associated with the entanglement structure of a quantum many-body state which may occasionally differ from the one suggested by the Hamiltonian of the system. Yet, the obtention of these entanglement links is a complex mathematical problem. In this work, we address this issue and propose several approximation techniques for matrix product states, free fermionic states, or in cases in which contiguous blocks are specially relevant. Along with this, we discuss the accuracy of the approximation for different types of states and partitions. Finally, we employ the link representation to discuss two different physical systems: the spin-1/2 long-range XXZ chain and the spin-1 bilinear biquadratic chain.

## I. INTRODUCTION

Entanglement is a key feature for the new developments in quantum physics. It constitutes the main resource for quantum technologies [1], characterizes the different phases of quantum matter [2, 3], and has been proposed as the building block of the fabric of space-time through the holographic principle and tensor networks [4–10]. This last conjecture derives from the so-called *area law*, which states that the entanglement entropy of a block of a low-lying energy eigenstate of a local Hamiltonian is proportional to the measure to its boundary [11–14], sometimes presenting logarithmic corrections [15–18]. Interestingly, there are relevant exceptions to the area law, such as the *rainbow state* [19–28]. In this case, despite the locality of the Hamiltonian, the ground state establishes long-range bonds between opposite sites of a chain, suggesting the possibility that the geometric structure described by the entanglement differs from the one associated to the Hamiltonian. Thus, given a quantum state, we are naturally led to the question: what is the geometry associated to its entanglement structure? A tentative answer to that question was provided by our group in [29], and we will build upon that work in order to provide a deeper insight.

The main insight in [29] is the *link representation* for the entanglement entropies (EE) of all the bipartitions of a given quantum state. A quantum system consisting of  $N$  parties (qubits or otherwise) will be represented by a link matrix,  $\{J_{ij}\}$ , with  $i, j \in \{1, \dots, N\}$ , with the property that the entanglement entropy of *any subsystem*  $A$  can be approximately computed as a sum of  $J$ -entries, also called *link strengths*, associated to all pairs of sites separated by the partition. In equation form

$$S_A \approx \sum_{\substack{i \in A, \\ j \in \bar{A}}} J_{ij}, \quad (1)$$

with  $J_{ij} \geq 0$ . The link matrix may be regarded as an *adjacency matrix* associated to the entanglement structure:  $J_{ij} > 0$  whenever there exists a connection between sites  $i$  and  $j$ . Thus, the geometry associated to entanglement can be directly read from the link matrix. In [29], we provided an algorithm to obtain the optimal entanglement links from the quantum state. In this work, we will address many relevant questions associated to the link representation of entanglement, such as the accuracy of the representation, efficient algorithms to obtain the entanglement links and their application to the analysis of quantum phases of matter.

This work is structured as follows. We provide a summary of known results in Sec. II. Then, we analyze the accuracy of the link representation in Sec. III. In section IV we will discuss different *approximation schemes* in order to obtain the link matrix. Indeed, the optimal algorithm shown in [29] takes exponential time in  $N$ . Thus, we will show more efficient approaches for matrix product states (MPS), free fermionic states and the case in which contiguous blocks are specially relevant, among others. Some physical applications to the analysis of long-range Hamiltonians and the Haldane phase are provided in Sec V. We conclude with a summary of our main conclusions and proposals for further work.

## II. LINK REPRESENTATION OF ENTANGLEMENT

This section reviews the main results of Ref. [29], with a slight improvement of the notation and the presentation.

Let us consider a pure state  $|\psi\rangle$  of  $N$  parties, which will be qubits in the simplest case. There exist  $2^N - 2$  possible subsystems (excluding the block with all sites and no sites),  $A$ , and for each of them the entanglement entropy (EE) can be defined as the von Neumann entropy associated to the reduced density matrix,

$$S_A = -\text{Tr}_A(\rho_A \log \rho_A), \quad (2)$$

with

$$\rho_A = \text{Tr}_{\bar{A}}|\psi\rangle\langle\psi|, \quad (3)$$

where  $\text{Tr}_A$  stands for the partial trace over subsystem  $A$ . Alternatively, different definitions of the EE can be employed, such as the set of Rényi entropies. Now as for any pure state,  $S_A$  obtained for one such subsystem and its complement yields the same entropy, the number of subsystem we actually need to consider is  $N_{\text{tot}} = 2^{N-1} - 1$ . Let  $I \in \{1, \dots, N_{\text{tot}}\}$  index the different subsystems through their binary expansion, and let us evaluate the EE for all of them,  $\mathcal{S} \equiv \{S_I\}_{I=1}^{N_{\text{tot}}}$ , which we will call the *full entropy data*.

Eq. (1) can be understood as a linear system of  $N_{\text{tot}}$  equations (one per  $S_I$ ) to determine  $N(N-1)/2$  unknowns, the link strengths. The system can be formally written as

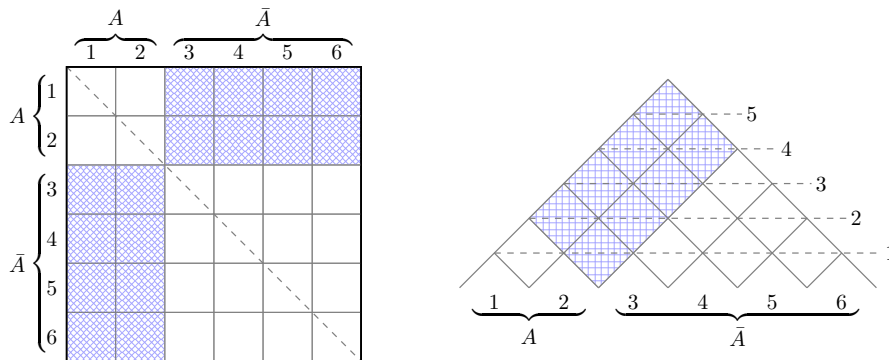


Figure 1: Link representation of the EE associated to the partition  $A = \{1, 2\}$ ,  $\bar{A} = \{3, 4, 5, 6\}$ . Left: link matrix representation, the shadowed entries must be added up to build  $S_A$ . Notice the mirror symmetry across the main diagonal. Right: triangular view of the link matrix, lying on the main diagonal. Horizontal lines correspond to different lengths for the associated links. Thus, the first level corresponds to links connecting neighboring sites,  $J_{1,2}$ ,  $J_{2,3}$ , etc. The link strengths that must be summed can be obtained in the following way. The EE of  $A$  or  $\bar{A}$  is obtained adding up all link strengths except the right-angled triangles over  $A$  and  $\bar{A}$ .

$$\mathcal{A}\mathcal{J} = \mathcal{S}, \quad (4)$$

where  $\mathcal{J}$  stands for the vector of  $N(N-1)/2$  link strengths, and  $\mathcal{A}$  is a matrix with combinatorial origin, whose entry  $\mathcal{A}_{Ik} = 1$  iff subsystem  $I$  breaks link  $k$ , or zero otherwise. Notice that the system (4) is overdetermined, since the number of equations is vastly superior to the number of unknowns, and in general it has no solutions. Yet, approximate solutions are still interesting. For example, we can obtain the optimal solution in the least-squares sense through the normal equations,

$$\mathcal{A}^\dagger \mathcal{A}\mathcal{J} = \mathcal{A}^\dagger \mathcal{S}. \quad (5)$$

These normal equations can be efficiently solved, since they are a set of  $N(N-1)/2$  equations with the same number of unknowns, yet the obtention of  $\mathcal{A}^\dagger \mathcal{S}$  requires the knowledge of the full entropy data. Solving Eq. (5) provides the *optimal link representation* for the associated full entropy data. We denote the  $J$ -matrix obtained in this way as  $J^{\text{opt}}$  that we shall use later on.

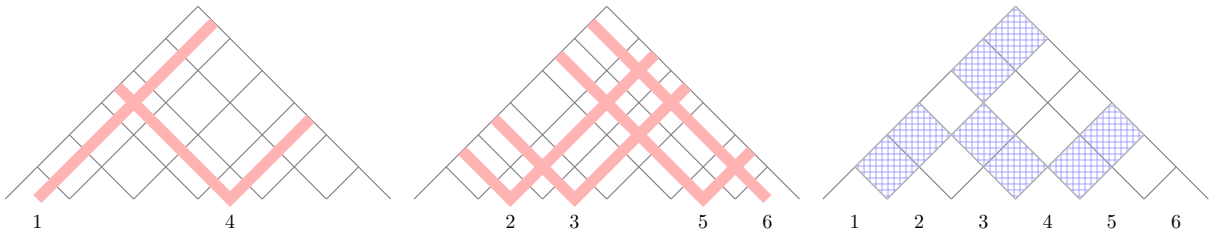


Figure 2: Understanding the triangle view of the link representation. In order to find the link strengths that must be added to find the EE of a certain partition we draw the *light cone* of all sites in  $A = \{1, 4\}$  (left), then of all sites in  $\bar{A} = \{2, 3, 5, 6\}$  (center). The intersection corresponds to the link strengths that contribute to  $S_A = S_{\bar{A}}$ .

### A. Entropies from link matrices

Fig. 1 provides an illustration to show how to read the EE of a region following Eq. (1). On the left we see the rectangular view of the link matrix for the block  $A = \{1, 2\}$ , shading the link strengths that contribute to  $S_A$ . On the right we can see a triangle view of the link matrix, based on the main diagonal. This representation makes the symmetry  $J_{ij} = J_{ji}$  manifest. Moreover, the height of a link strength above the base line corresponds to the length of the corresponding link.

In Fig. 2 we provide an alternative route to obtain the link strengths contributing to the EE of a certain subsystem  $A$ . From each site in  $A$  we can draw the *light cone* by tracing two diagonal lines at 45 degrees. The light cone of a site corresponds to the links which start at the given site. The link strengths to be added are just the intersection of the light cone of  $A$  and that of  $\bar{A}$ .

The link representation of the EE has a series of properties which have been rigorously proved in [29]: (a) Symmetry,  $S_A = S_{\bar{A}}$ , which is exact for pure states; (b) Subadditivity:  $S_A + S_B \geq S_{AB}$ , which implies the positivity of the mutual information,  $I(A : B) \equiv S_A + S_B - S_{AB}$ ; (c) Strong subadditivity,  $S_{AB} + S_{BC} \geq S_{ABC} + S_B$ .

### B. Some exact cases

The link representation is exact for valence bond states (VBS). For example, a dimerized state creating bonds between sites  $2i$  and  $2i + 1$  will have link strengths  $J_{2i, 2i+1} = \log 2$  and zero otherwise. The rainbow state, which can be obtained in the strong inhomogeneity limit from local 1D Hamiltonians is a VBS linking site  $i$  and  $N + 1 - i$ , has link strengths  $J_{i, N+1-i} = \log 2$  and zero otherwise. In these cases, the EEs of all partitions are exactly obtained through the link representation. Conformal states in (1+1)D have a link representation, in which  $J(x, y) = (c/6)/(x - y)^2$  where  $c$  is the central charge and  $x, y$  run over the real line. In the continuum limit we must introduce a short distance regulator  $\epsilon > 0$ , and define the intervals as  $A_\epsilon = (\epsilon/2, \ell - \epsilon/2)$  and  $\bar{A}_\epsilon = (-\infty, -\epsilon/2) \cup (\ell + \epsilon/2, \infty)$ , thus obtaining

$$S_{A_\epsilon} \simeq \int_{A_\epsilon} dx \int_{\bar{A}_\epsilon} dy \frac{c/6}{(x - y)^2} = \frac{c}{3} \log \frac{\ell}{\epsilon}. \quad (6)$$

Indeed, the link strength  $J_{ij}$  has an interesting interpretation from the conformal field theory (CFT) point of view, as the correlation function of two currents,  $J(x, y) = \langle \mathbf{J}(x) \mathbf{J}(y) \rangle$ .

### C. Link representation and mutual information

Let us remind the definition of mutual information between two subsystems  $A$  and  $B$ ,

$$I(A : B) \equiv S_A + S_B - S_{AB} \geq 0, \quad (7)$$

which can be obtained easily within the link representation,

$$I(A : B) = 2 \sum_{\substack{i \in A, \\ j \in B}} J_{ij}. \quad (8)$$

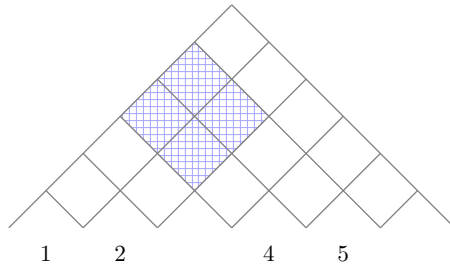


Figure 3: Triangle view of the link representation of the mutual information  $I(A : B)$  between two intervals,  $A = \{1, 2\}$  and  $B = \{4, 5\}$ , as the diamond spanned by them.

If  $A = \{i\}$  and  $B = \{j\}$  we see that  $I(i : j) = 2J_{ij}$ , thus providing a direct physical interpretation for  $J_{ij}$ . Interestingly, the graphical representation of the mutual information between two subsystems is simpler than for the EE, as it can be checked in Fig. 3.

#### D. Entanglement contour

An *entanglement contour* associated to a given subsystem is a partition of the EE among its sites [30] (see also [31, 32]),  $s_A(i) \geq 0$ , such that  $\sum_i s_A(i) = S_A$ . The link representation provides an entanglement contour for each possible subsystem,

$$s_A(i) = \sum_{j \in \bar{A}} J_{ij}. \quad (9)$$

Notice that, in similarity to the link representation, the entanglement contour is not uniquely defined. Indeed, the contour for a single block  $A$  is *underdetermined*, i.e. there are many possible contours  $\{s_A(i)\}_{i=1}^{|A|}$  yielding the same EE  $S_A$ . Yet, physically motivated definitions tend to coincide [24, 25].

### III. ACCURACY OF THE LINK REPRESENTATION

The accuracy of the optimal link representation, given by the solution of Eq. (5), can be quantified as follows. Let us obtain the EE of all blocks within the link representation,  $\{\hat{S}_I\}_{I=1}^{N_{\text{tot}}}$ , and then compare these values to the exact ones,  $\{S_I\}_{I=1}^{N_{\text{tot}}}$ , obtaining the average absolute error,

$$\Delta S \equiv \frac{1}{N_{\text{tot}}} \sum_I |\hat{S}_I - S_I|. \quad (10)$$

This average error can be properly normalized dividing each partition error by its entropy, giving rise to the average relative error,

$$\Delta_R S \equiv \frac{1}{N_{\text{tot}}} \sum_I \frac{|\hat{S}_I - S_I|}{S_I}. \quad (11)$$

Yet, this definition is not very convenient, because some EE can be exactly zero. Thus, it is more relevant to define the *average EE* over all partitions,  $\langle S \rangle$ , and use it to define a relative error

$$\varepsilon = \frac{\Delta S}{\langle S \rangle}. \quad (12)$$

On occasions, it is also convenient to restrict the error measure over some subset of partition. In this case, we will use a suitable notation to highlight that we are not extending the measure to the full entropy data.

As a benchmark, we will employ two reference states: the ground state (GS) of a conformally invariant free-fermionic state, and a random state.

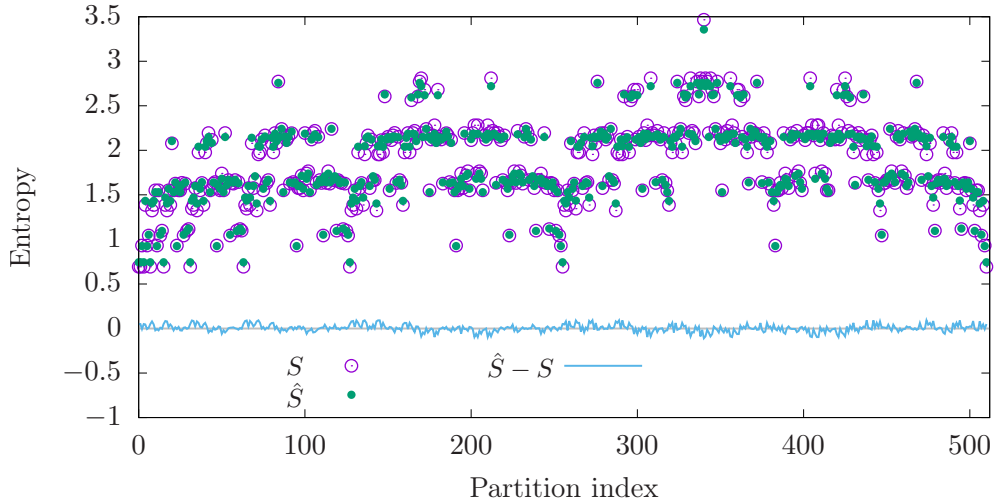


Figure 4: Entropies of all subsystems, in lexicographical order, along with the (signed) absolute errors associated to the optimal link representation for free fermion state with  $N = 10$  sites. Here the empty circles correspond to the exact values of the entropies,  $S_I$ , while the full dots correspond to the optimal values obtained using the link representation,  $\hat{S}_I$ .

### A. Free fermionic states

Let us consider the Hamiltonian

$$H = - \sum_i t_{i,i+1} c_i^\dagger c_{i+1} + \text{h.c.}, \quad (13)$$

where  $c_i$  is the fermionic annihilation operator on site  $i$  with either open boundary conditions (OBC) or periodic (PBC), in this case using only  $N = 2 \bmod 4$  to avoid degeneracies. The GS of this Hamiltonian is a Slater determinant, which can be written as  $|\Psi\rangle = \prod_{k=1}^{N/2} b_k^\dagger |0\rangle$ , with  $b_k^\dagger = \sum_i U_{k,i} c_i^\dagger$  and  $U$  is the matrix diagonalizing the hopping matrix  $UTU^\dagger = \tilde{T}$ , with  $T_{i,i+1} = T_{i+1,i} = t_{i,i+1}$ . We should stress that the free fermionic GS with  $t_{i,i+1} = 1$  does not follow a strict area law. Instead, the entanglement entropy of a contiguous block of size  $\ell$  grows like  $S(\ell) \approx (c/3) \log \ell$ , due to conformal invariance. We will also consider a dimerized Hamiltonian,

$$H = - \sum_i (1 + (-1)^i \delta) c_i^\dagger c_{i+1} + \text{h.c.}, \quad (14)$$

which is not conformally invariant, and presents a mass gap.

Fig. 4 shows the entropies for all partitions of the free fermion state with  $t_{i,i+1} = t$  and  $N = 10$  sites. Actually, not all the subsystems are shown, because due to the symmetry  $A \leftrightarrow \bar{A}$ , we may disregard those with the last site absent, thus retaining only  $N_{\text{tot}} = 2^{N-1} - 1$ . The empty circles correspond to the exact values of the entropies,  $S_I$ , while the full dots correspond to the optimal values obtained using the link representation,  $\hat{S}_I$ . The continuous line below shows the signed absolute error,  $\hat{S}_I - S_I$ , which averages to zero.

Notice that absolute errors shown in Fig. 4 are very tiny. Indeed, the average relative error, as defined in Eq. (12), is 1.7%. Are there any systematic trends for different types of blocks? Indeed, Fig. 4 presents noticeable patterns. Some blocks of neighboring entropies present negligible error, while other groups present larger deviations. Fig. 5 clusters the data as a function of the number of sites (left) and the number of blocks (right) in each partition. Regarding the dependence of the error on the number of sites,  $\ell$  we observe that the natural symmetry  $\ell \leftrightarrow N - \ell$  is respected. The relative error is lowest for number of sites close to  $N/2$ . The reason is that the optimal link representation attempts to fit all entropy data simultaneously, and the number of partitions with  $\ell \sim N/2$  is higher than for either small or large sizes. On the other hand, we observe that the relative error is approximately constant for all block sizes, even though the absolute error grows with the number of blocks.

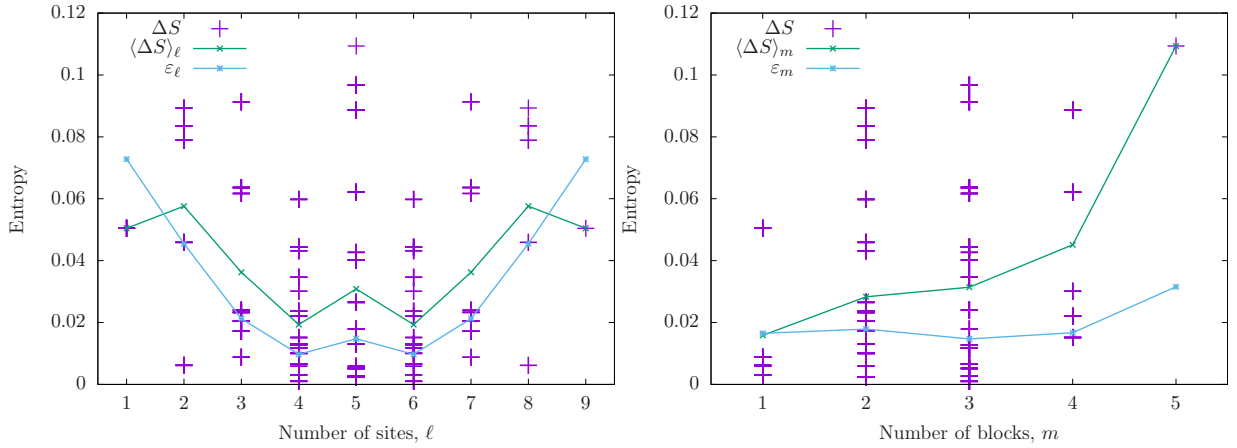


Figure 5: Accuracy of the link representation for the free fermionic state. Left: the purple crosses represent the entropy absolute errors classified by the number of sites in our block, the green line denotes the average of this absolute error for each block size, and the cyan line divides this value by the average entropy corresponding to each block size, yielding a relative error. Right: same data, classified by the number of blocks in each partition.

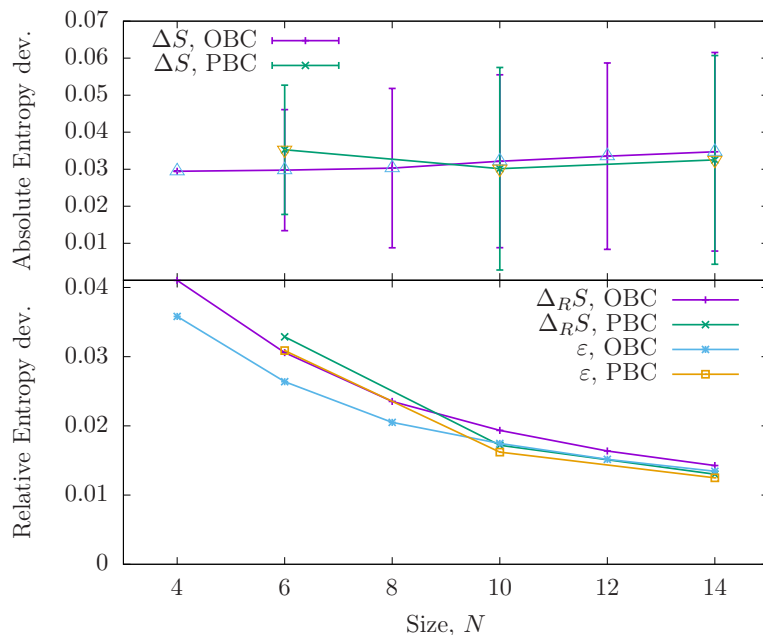


Figure 6: Top: Absolute mismatch between the exact and the approximate entropies of the GS of fermionic chains with OBC and PBC, along with their deviations, for different system sizes. Bottom: Relative mismatch between the exact and approximate entropies, along with the error defined in Eq. (12).

## B. Size dependence

It is important to ask how does the accuracy of the link representation scale with the system size. Unfortunately, Eq. (5) can not be solved for large system sizes. We have obtained the absolute and relative deviations, Eq. (10) and (11) along with the *error* defined through Eq. (12) for the GS of open and periodic fermionic chains up to  $N = 14$ . In the periodic case, we have restricted the computation to values of  $N = 2 \bmod 4$ , because only in that case the GS is unique. The results are shown in Fig. 6.

We observe that though the absolute error remains almost constant, the relative errors decay as a function of the system size, thus showing that the optimal link representation gets more and more accurate as the system size increases. These results suggest that the optimal link representation may become exact in the thermodynamic limit for these conformally invariant states. Unfortunately, the huge computational effort required to obtain the optimal

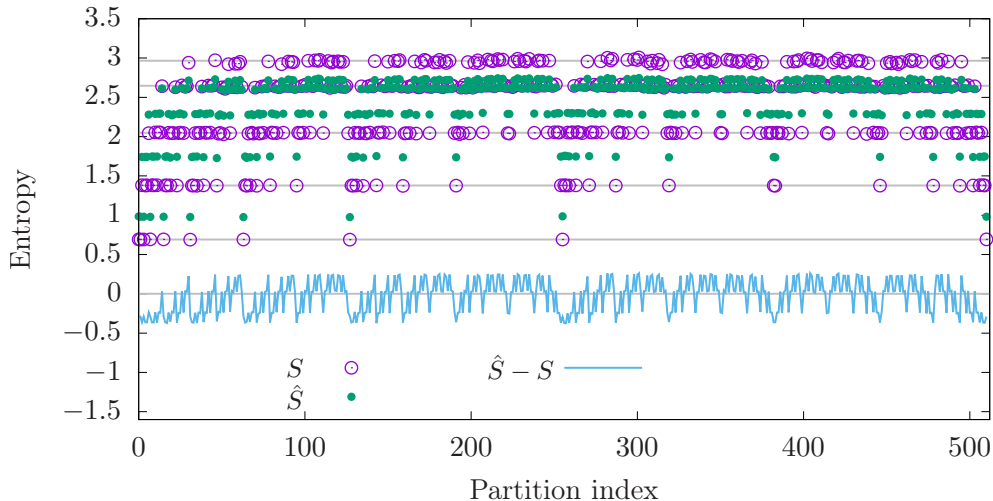


Figure 7: Entropies of all subsystems, in lexicographical order, along with the (signed) absolute errors associated to the optimal link representation for a realization of the random state defined in the text. Here the empty circles correspond to the exact values of the entropies,  $S_I$ , while the full dots correspond to the optimal values obtained using the link representation,  $\hat{S}_I$ . The horizontal bars mark the expectation values for the entropies according to Page's law for each block size, following Eq. (15).

link representation forces us to attempt alternative approximations.

### C. Random states

Let us consider random pure states of  $N$  qubits under a Haar measure. They can be sampled by choosing the real and imaginary parts of each component on any basis from a standard Gaussian distribution, and normalizing afterwards. The entanglement entropy of these states has been known for a long time [33]. Indeed, it was shown that the average entropy of a subsystem only depends on the minimum between the number of sites of the aforementioned subsystem and those of the complementary,

$$\langle S(\ell) \rangle \approx \ell \log 2 - \frac{1}{2^{N-2\ell+1}}. \quad (15)$$

Naturally, these averages are taken for many states and subsystems. Yet, a single realization shows the remarkable accuracy of Eq. (15), as we can see in Fig. 7, where all the entropies of a single random state have been depicted in empty circles, as in Fig. 4, with the approximation according to the optimal link representation in full circles. The horizontal grey lines correspond to the theoretical predictions for the average of the entropy for each block size, Eq. (15). We notice that the exact values fluctuate weakly around the theoretical predictions, with larger fluctuations corresponding to larger sizes.

The relative errors are much higher than in the free fermionic case, around 7%. The approximate values obtained with the optimal link representation also appear in horizontal lines corresponding to block sizes, but these lines do not correspond to the exact ones. The effective permutation invariance of the state gives rise to nearly constant link strengths,  $J_{ij} \approx \chi$  for all  $i, j$ . In our case, we obtain  $\chi = 0.157 \pm 0.004$ . The prediction for the entropy of a block of size  $\ell$ , according to the optimal link representation is

$$S(\ell) = \chi \ell (N - \ell). \quad (16)$$

Obtaining the link representation for these states amounts to an attempt to fit Page's law using Eq. (16), as we can see in Fig. 8. For  $\ell \ll N$ , a better link representation is obtained by choosing  $\chi = N^{-1}$ .

Indeed, the link representation is not specially good for random states. The reason is that it has been designed for states for which *an area law* may emerge, either through the geometry of the Hamiltonian or a different geometry, associated to entanglement.

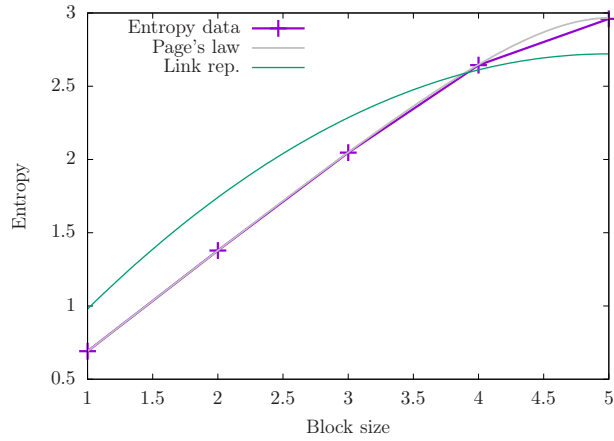


Figure 8: Comparison of the predictions of Page's law and the optimal link representation for the average entropies of a random state.

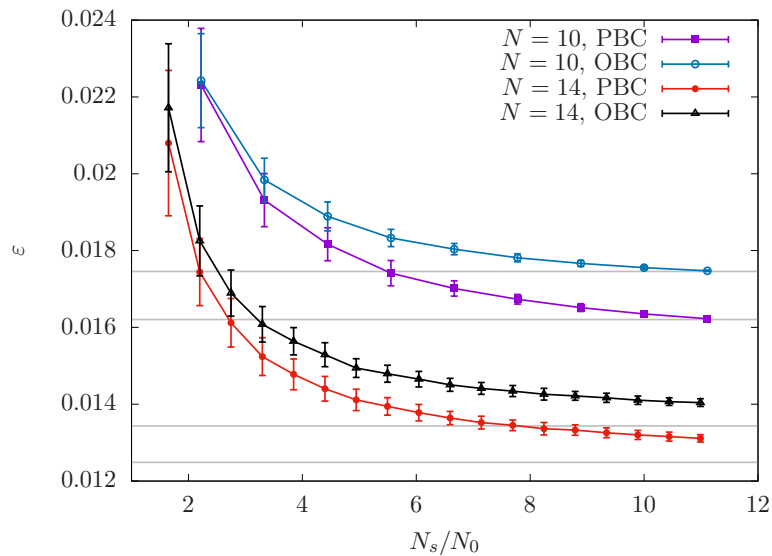


Figure 9: Error of the link representation obtained with  $N_s$  samples of the partition space, scaled with  $N_0 = N(N-1)/2$ , for four different fermionic GS, with OBC and PBC,  $N = 10$  and  $14$ . Gray lines correspond to the error associated to the optimal link representation, see Fig. 6.

#### IV. APPROXIMATION METHODS FOR THE ENTANGLEMENT LINKS

Obtaining the optimal link representation associated to a pure state is a hard computational problem, in general terms, since it requires the determination of the full entropy data, in principle  $2^N$  entropies, although it reduces in practice to  $N_{\text{tot}} = 2^{N-1} - 1$  independent values. Obtaining the EE of arbitrary partitions for arbitrary quantum states is a costly procedure itself. Thus, it is specially relevant to devise efficient approximation techniques. Ideally, that requires a polynomial amount of resources.

Finding an efficient approximation for the link matrix is not only a technical necessity. It is also a problem of fundamental relevance: can we obtain a link representation for GS of local Hamiltonians?

##### A. Random sampling

A first approximation scheme can be built renouncing to consider an exponential number of partition, and *sampling* a number  $N_s$  of them instead. The results are indeed promising. Of course,  $N_s$  must be larger than  $N(N-1)/2 \equiv N_0$ , which is the number of independent link strengths. Fig. 9 shows the average error associated to the link representation



obtained sampling  $N_s$  partitions, as a function of  $N_s/N_0$  for two fermionic GS, with open and periodic boundaries (OBC and PBC) and two sizes,  $N = 10$  and  $N = 14$ , with the associated error bars. The horizontal lines correspond to the errors associated to the optimal link representation. Each experiment was repeated 100 times in order to ensure reproducibility of our results.

From Fig. 9 we are led to conjecture that for a state with a good link representation, sampling  $N_s \approx 10 \times N_0$  should be enough for reasonably accurate values of the link strengths. This is indeed good news, since it means that we should obtain the entropies of  $O(N^2)$  partitions and solve a linear system of a similar size, thus rendering the problem tractable.

### B. Entanglement links for contiguous blocks

Let us consider the possibility that we do not have access to the full entropy data, but only the EE corresponding to contiguous blocks on a length  $N$  chain with PBC. A proper notation can be rather helpful. Let us define

$$A_{i,j} = \{i, \dots, j-1\}, \quad (17)$$

where site indices are always considered mod  $N$ , and  $S_{i,j} = S[A_{i,j}]$  is the associated EE. Thus,  $S_{i,i} = 0$  for any pure state, because  $A_{i,i}$  is always the whole chain. Moreover,  $S_{i,i+1}$  stands for the EE of block  $A_{i,i+1} = \{i\}$ . Naturally, for a pure state we have  $S_{i,j} = S_{j,i}$ , because both blocks are complementary, and this symmetry property motivates the definition.

The entropies  $S_{i,j}$  can be expressed through

$$S_{i,j} = \sum_{k=i}^{j-1} \sum_{l=j}^{i-1} J_{k,l}, \quad (18)$$

where the summations must be understood mod  $N$ . Let us obtain its difference in the first index,

$$(\Delta_1 S)_{i,j} \equiv S_{i+1,j} - S_{i,j} = \left( \sum_{k=i+1}^{j-1} - \sum_{k=j}^i \right) J_{i,k}, \quad (19)$$

and now, let us obtain its difference in the second index,

$$\begin{aligned} (\Delta_2 \Delta_1 S)_{i,j} &= (\Delta_1 S)_{i,j+1} - (\Delta_1 S)_{i,j} \\ &= \left( \sum_{k=i+1}^j - \sum_{k=j+1}^i - \sum_{k=i+1}^{j-1} + \sum_{k=j}^i \right) J_{i,k} \\ &= S_{i+1,j+1} - S_{i+1,j} - S_{i,j+1} + S_{i,j} \\ &= 2J_{i,j}. \end{aligned} \quad (20)$$

The continuous version of this equation is simply

$$J(x,y) = \frac{1}{2} \frac{\partial^2 S(x,y)}{\partial x \partial y}, \quad (21)$$

where we have assumed that  $S(x,y)$  is the EE of the interval  $[x,y]$ . The validity of Eq. (20) can be checked graphically in Fig. 15 in Appendix A.

Notice that the equation of  $2J_{i,i+1} = S_{i+1,i+2} - S_{i+1,i+1} - S_{i,i+2} + S_{i,i+1} = S[i] + S[i+1] - S[i,i+1]$ , i.e. it is the mutual information between the neighboring sites. For longer links this equation is not valid. Moreover, in the case of a translation invariant state Eq. (20) reduces to

$$J_{i,i+r} = S(r) - \frac{1}{2}S(r-1) - \frac{1}{2}S(r+1), \quad (22)$$

| $n_B$ | $\varepsilon$ |          |          |
|-------|---------------|----------|----------|
|       | $N = 6$       | $N = 10$ | $N = 14$ |
| 1     | 0.0611        | 0.0663   | 0.0681   |
| 2     | 0.0272        | 0.0281   | 0.0362   |
| 3     | 0.0308        | 0.0173   | 0.0187   |
| 4     |               | 0.0161   | 0.0133   |
| 5     |               | 0.0162   | 0.0125   |
| 6     |               |          | 0.0124   |
| 7     |               |          | 0.0124   |

Table I: Relative errors within the structured approximation, as a function of the number of blocks considered in the partition for a free-fermionic GS with PBC.

where  $S(r)$  denotes the EE of all contiguous blocks of size  $r$ . In the continuous limit, Eq. (22) becomes

$$J(\ell) = -\frac{1}{2} \frac{\partial^2 S(\ell)}{\partial \ell^2}. \quad (23)$$

These two last equations were already shown in Ref. [29].

We may generalize the above expression in order to build an approximation to the entanglement links which only considers partitions containing  $n_B$  contiguous blocks or less. Thus, the aforementioned contiguous block approximation would correspond to the  $n_B = 1$  case. Naturally, the quality of this approximation will grow with  $n_B$  up to the maximal value,  $n_B = N/2$ . Table I shows the relative errors associated to this structured approximation for a free-fermionic GS with PBC.

### C. Approximation for free-fermionic states

Let us consider a Gaussian fermionic state, written in the form of a Slater determinant,  $|\Psi\rangle = \prod_k b_k^\dagger |0\rangle$ , with  $b_k^\dagger = \sum_i U_{k,i} c_i^\dagger$ , where  $c_i^\dagger$  is the creation operator on the  $i$ -th site. The entanglement properties associated to a block  $A$  can be obtained through the correlation submatrix,  $(C_A)_{i,j} = \sum_k \bar{U}_{k,i} U_{k,j}$ , with  $i, j \in A$ . Let  $C_A = W_A \Lambda_A W_A^\dagger$ , where  $\Lambda_A = \text{diag}(\nu_1^A, \dots, \nu_{|A|}^A)$ . Then,

$$S_A = \sum_{p=1}^{|A|} H_2(\nu_p), \quad (24)$$

where  $H_2(x) \equiv -x \log(x) - (1-x) \log(1-x)$ . Interestingly, the eigenvectors of  $C_A$ , given in the columns of  $W_A$ , are usually disregarded, except in the evaluation of the *entanglement contour*, which provides a possible partition of the EE among the different sites of the block,

$$s_A(i) = \sum_{p=1}^{|A|} H_2(\nu_p) |(W_A)_{p,i}|^2, \quad (25)$$

from which it is clear that  $s_A(i) \geq 0$  and  $\sum_{i \in A} s_A(i) = S_A$ . Let us also consider the complementary block,  $\bar{A}$ . Indeed,  $\Lambda_A$  and  $\Lambda_{\bar{A}}$  are easily related: for every eigenvalue  $\nu_p^A \in (0, 1)$  there must be corresponding eigenvalue  $\nu_{q(p)}^{\bar{A}} = 1 - \nu_p^A$ . Barring degeneracies, each eigenvector  $(W_A)_p$  of  $C_A$  corresponds to an eigenvector of  $(W_{\bar{A}})_{q(p)}$  of  $C_{\bar{A}}$ , and we may write the approximation

$$J_{i,j} \simeq \sum_{p=1}^{|A|} H_2(\nu_p^A) |(W_A)_{p,i} (W_{\bar{A}})_{q(p),j}|^2. \quad (26)$$

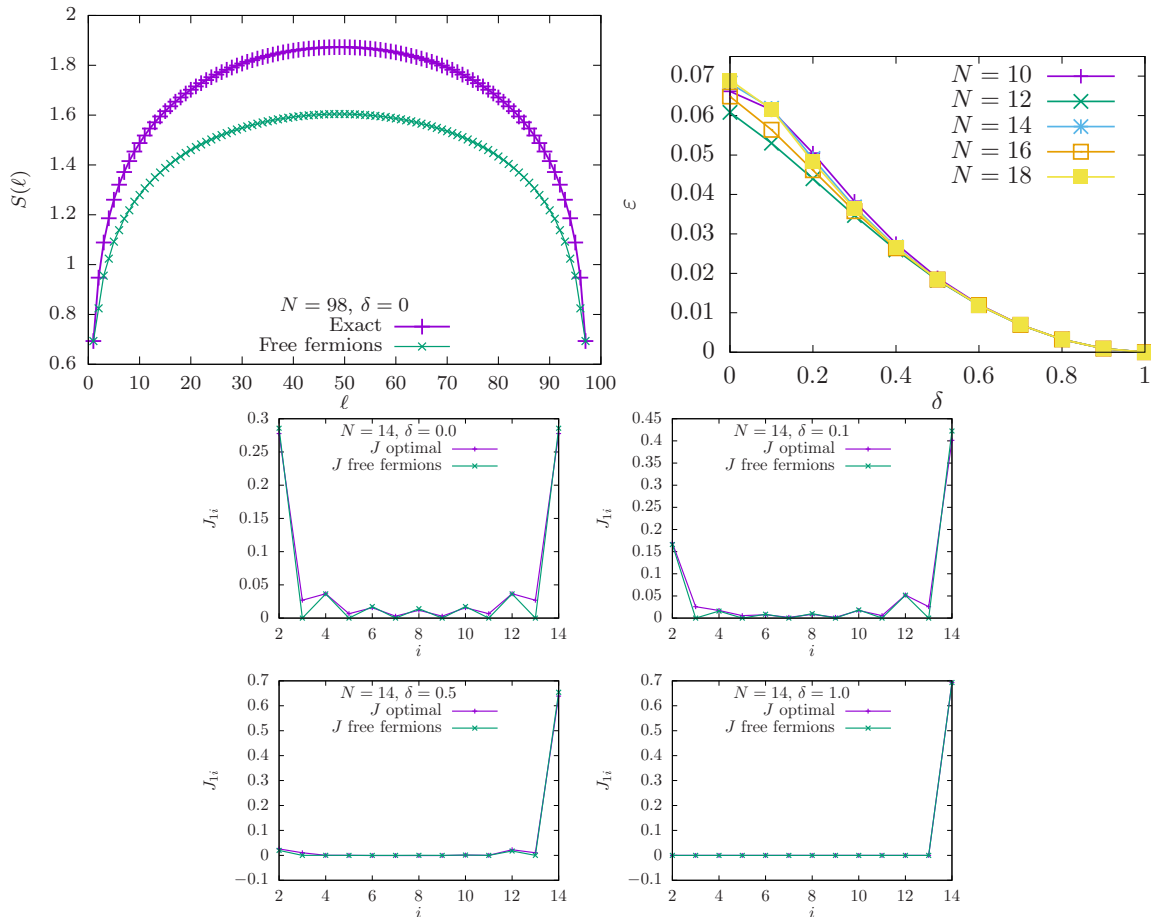


Figure 10: (a) Entropies  $S[1, \dots, \ell]$  as a function of  $\ell$  for the same system, comparing with the compact-block approximation and the free-fermionic approximation for a chain with  $N = 98$  sites, which is clearly not accurate. (b) Error of the free-fermionic approximation as a function of  $\delta$  for several sizes. Notice that they are approximately equal, and decay to zero as  $\delta$  increases. (c) Values of  $J_{i,i+n}$  for a dimerized free-fermionic chain as a function of  $n$  for several values of  $\delta$ . Notice that the even values are correctly represented, but not the odd ones, which are zero in the free-fermionic approximation.

In similarity with the equation for the entanglement contour, Eq. (25), Eq. (26) obtains the entanglement links by partitioning the entanglement entropy into contributions stemming from pairs of sites. In practice, Eq. (26) presents several drawbacks. First, the entanglement links obtained correspond to a single partition. A possible solution is to consider a finite set of partitions and average the values of the entanglement links over them. Moreover, the spectrum  $\{\nu_p^A\}$  is very often exactly degenerate, thus preventing us from a clear association between the eigenvalues of  $A$  and  $\bar{A}$ .

These drawbacks lead us to propose a concrete application for the simplest case, where we consider the set of partitions containing a single site,  $A_i = \{i\}$ . In this case, the spectrum of  $C_{A_i}$  contains a single entry,  $C_{i,i}$ , and the spectrum of  $C_{\bar{A}_i}$  contains a single non-trivial entry,  $1 - C_{i,i}$ . Thus, we can write

$$J_{i,j} = \frac{1}{2} (H_2(C_{i,i})|B_{i,j}|^2 + H_2(C_{j,j})|B_{j,i}|^2), \quad (27)$$

where  $B_{i,j} = (W_{\bar{A}_i})_{q,j}$  is the  $j$ -th component of the eigenvector associated to the single non-trivial eigenvalue of  $C_{\bar{A}_i}$ . The advantage of this approach is its extreme simplicity and low computational cost.

We should remark that this approximation is exact for partitions containing a single site, but for other blocks the accuracy can be much less than that obtained for the optimal link matrix. Indeed, as we shall show, the EE of large contiguous blocks can be subject to larger errors, while the global accuracy is still good enough because of the large number of sparse partitions.

The top-left panel of Fig. 10 shows the EE of a contiguous block starting from the left for a periodic fermionic chain with  $N = 98$ , obtained within the contiguous blocks approximation (which is exact in this case by construction)

and for the free-fermionic approximation. Indeed, the error for those EE is large. In order to understand why we may take a look at the bottom panel of Fig. 10, where we see the optimal link strengths compared to the free-fermion approximation for different distances,  $J_{i,i+n}$ . The most striking difference is the fact that the exact link strengths for odd  $n$  are non-zero, but the free-fermionic approximation is zero. The non-zero values of  $J_{i,i+n}$  are very accurately obtained with the free-fermionic approximation. Thus, we are led to the conjecture that the free-fermionic approximation imposes a structure on the link representation which is not optimal, related to the parity oscillations associated to the Fermi momentum  $k_F = \pi/2$ .

The top-right panel of Fig. 10 provides some good news regarding the relative error associated to the free-fermionic link representation for different sizes of the dimerized GS, Eq. (14), as a function of  $\delta$ . We notice that the error is a few percent for  $\delta \rightarrow 0$ , several times larger than the optimal value, and nearly independent of the system size  $N$ . As  $\delta$  increases, the error is reduced, and for large  $\delta$  we approach a valence bond state for which the error vanishes. Since this representation is extremely cheap to obtain, in terms of computational resources, it seems to be a good choice only for states which are close to a VBS.

#### D. Approximation for matrix product states

Matrix product states provide the main examples for states fulfilling the area law of entanglement. Therefore, we expect them to have a specially simple link representation, with exponentially decaying link strengths,  $J_{i,j} \approx \exp(-|i-j|/\xi)$ , for some correlation length  $\xi$  [34]. Indeed, this is our main result, but the technical details are also relevant. We will provide explicit expressions for the link strengths based on two different approximations. First, as we mentioned before, the link strengths can be approximated as the mutual information between pairs of sites. Then, we will approximate the link strengths from the entropies of contiguous blocks, via Eq. (22).

##### 1. Mutual information approximation

Let us consider a translational invariant matrix product state (MPS) representation of a general quantum many-body state  $|\Psi\rangle$  with periodic boundary condition [35–37], given by

$$|\Psi\rangle = \sum_{i_1 i_2 \dots i_N} \text{Tr}(A_{i_1} A_{i_2} \dots A_{i_N}) |i_1 i_2 \dots i_N\rangle, \quad (28)$$

where  $A_{i_k}$  are  $D \times D$  matrix. Now starting from the above expression our aim is to find the reduced density matrix corresponding to the block formed by sites  $i$  and  $j$ , situated at a distance  $l + 1 = |j - i|$  from each other. In other words, we wish to compute

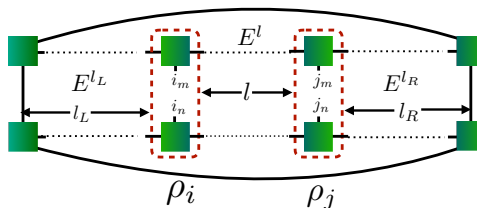


Figure 11: Schematic illustration of the few-site reduced density matrix obtained from a periodic MPS by contraction of tensors.  $\rho_i$  and  $\rho_j$  denote single-site density matrices which are situated at a distance of  $l$  sites from each other and  $E$  is the transfer matrix.

$$\rho_{ij} = \text{Tr}_{\overline{\{i,j\}}} |\Psi\rangle\langle\Psi|. \quad (29)$$

Let us express the above computation in the language of the transfer matrix  $E = \sum_{i_k} A_{i_k} \otimes A_{i_k}^*$ , where  $A^*$  is the complex conjugate of  $A$ , and let us make use of its representations in left and right eigenvectors  $E = \sum_{s=0}^{D^2-1} \gamma_s |R_s\rangle\langle L_s|$ . The two-site reduced state can be written as

$$\rho_{ij} = \rho_i \otimes \rho_j + \gamma_1^l \bar{\rho}_{ij}, \quad (30)$$

where  $\gamma_1$  is the second highest eigenvalue of the transfer matrix,

$$\begin{aligned} \rho_i &= \sum_{i_m j_m} \langle L_0 | A_{i_m} \otimes A_{i_m}^* | R_0 \rangle | i_m \rangle \langle i_m |, \\ \rho_j &= \sum_{i_n j_n} \langle L_0 | A_{j_n} \otimes A_{j_n}^* | R_0 \rangle | j_n \rangle \langle j_n |, \end{aligned} \quad (31)$$

and we denote (for  $l_L + l_R \gg 1$ , see Fig. 11)

$$\bar{\rho}_{ij} = \sum_{i_m i_n j_m j_n} \langle L_0 | A_{i_m} \otimes A_{i_n}^* | R_1 \rangle \langle L_1 | A_{j_m} \otimes A_{j_n}^* | R_0 \rangle.$$

(See Appendix B for the derivation.) Note here that the two matrices  $\rho_i$  and  $\rho_j$  in Eq. (31) are the same, but defined in the local Hilbert spaces of the sites  $i$  and  $j$ . Moreover, we have assumed the canonical form of the  $A_{i_k}$  matrices (right or left canonical), which yields a unique highest value of  $\gamma_s$ ,  $|\gamma_0| = 1$  and all other  $\gamma_s$ 's are arranged according to the decreasing value of their modulus.

To compute the entropy function  $S(\rho_{ij})$ , we have to take the logarithm of  $\rho_{ij}$ . Let us denote  $\rho_{ij}^0 = \rho_i \otimes \rho_j$ . Now let us consider the most general case, when  $\rho_{ij}^0$  and  $\bar{\rho}_{ij}$  do not commute. In that case, the expansion of the logarithm goes as follows.

$$\begin{aligned} \log(\rho_{ij}) &= \log(\rho_{ij}^0 + \gamma_1^l \bar{\rho}_{ij}) \\ &= \log(\rho_{ij}^0) + \gamma_1^l \int_0^\infty \frac{1}{\rho_{ij}^0 + z} \bar{\rho}_{ij} \frac{1}{\rho_{ij}^0 + z} dz - \gamma_1^{2l} \int_0^\infty \frac{1}{\rho_{ij}^0 + z} \bar{\rho}_{ij} \frac{1}{\rho_{ij}^0 + z} \bar{\rho}_{ij} \frac{1}{\rho_{ij}^0 + z} dz + O(\gamma_1^{2l+1}). \end{aligned} \quad (32)$$

The above expansion presents similarities to Dyson's equation for Green functions. Now using the above expansion we derive the approximate analytical expression of  $J_{ij}^{\text{mut}}$ , given by (see Appendix C for the complete derivation)

$$J_{ij}^{\text{mut}} = \frac{1}{2} (S(\rho_{ij}^0) - S(\rho_{ij})) = \frac{\gamma_1^l}{2} \text{Tr}(\bar{\rho}_{ij} \log(\rho_{ij}^0)) + \frac{\gamma_1^{2l}}{2} \left( \sum_m \frac{1}{2E_m} |\bar{\rho}_{ij}(mm)|^2 + \sum_{m \neq n} \left[ \frac{E_n}{(E_m - E_n)^2} \log \frac{E_n}{E_m} \right] |\bar{\rho}_{ij}(mn)|^2 \right), \quad (33)$$

where  $\bar{\rho}_{ij}$  is  $\bar{\rho}_{ij}$ , expressed in the eigenbasis of  $\rho_{ij}^0$ , and  $E_m$  are the eigenvalues of  $\rho_{ij}^0$ . Now using that  $\text{Tr} \bar{\rho}_{ij} = 0$ , one can show that the coefficient of  $\gamma_1^l$ ,  $\text{Tr}(\bar{\rho}_{ij} \log(\rho_{ij}^0)) = 0$ . Hence, finally we have

$$J_{ij}^{\text{mut}} = \frac{\gamma_1^{2l}}{2} \left( \sum_m \frac{1}{2E_m} \|\bar{\rho}_{ij}(mm)\|^2 + \sum_{m \neq n} \left[ \frac{E_n}{(E_m - E_n)^2} \log \frac{E_n}{E_m} \right] |\bar{\rho}_{ij}(mn)|^2 \right). \quad (34)$$

Therefore, the above equation implies that for the cases where the system admits a MPS form,  $J_{ij}^{\text{mut}}$  decays in general as a power of the second highest eigenvalue of the transfer matrix. The above relation holds even when the blocks  $i$  and  $j$  consists of more than one site. In that case one needs to compute  $\rho_{ij}^0$  and  $\bar{\rho}_{ij}$  accordingly. An example of such case is the AKLT state which exhibits a perfect area law when the blocks  $i, j$  are of sufficiently large and in that case  $J_{ij}^{\text{mut}}$  decays as  $(-1/3)^{2l}$ . Now one should note here that for a translationally invariant system, like the MPS considered above,  $J_{ij}^{\text{mut}} = J_{i+r, j+r}^{\text{mut}}$  for any  $r$ . To examine how close the values of  $J_{ij}^{\text{mut}}$  obtained in Eq. (34) remain to their exact value  $I_{ij}/2$  we have considered the GS of transverse field Ising model with periodic boundary condition, given by

$$H_{\text{Ising}} = - \sum_{i=1}^N \sigma_i^x \sigma_{i+1}^x - h_z \sum_{i=1}^N \sigma_i^z, \quad (35)$$

where  $\sigma_k^i$  are Pauli spin-1/2 operators at site  $k$ , and we compare  $J_{ij}^{\text{mut}}$  and  $I_{ij}/2$  for two different values of the transverse field  $h_z$  in Table II.

| $h_z$ | $l$ | $I_{1,2+l}/2$ | $J_{1,2+l}^{\text{mut}}$ | $h_z$ | $l$ | $I_{1,2+l}/2$ | $J_{1,2+l}^{\text{mut}}$ |
|-------|-----|---------------|--------------------------|-------|-----|---------------|--------------------------|
| 1.4   | 0   | 0.09776       | 0.09717                  | 2.0   | 0   | 0.05859       | 0.08080                  |
|       | 1   | 0.02693       | 0.02920                  |       | 1   | 0.00876       | 0.01161                  |
|       | 2   | 0.00889       | 0.00881                  |       | 2   | 0.00150       | 0.00167                  |
|       | 3   | 0.00310       | 0.00265                  |       | 3   | 0.00024       | 0.00024                  |
|       | 4   | 0.00134       | 0.00079                  |       | 4   | 0.00004       | 0.00003                  |

Table II: Comparing the link strengths  $J_{ij}^{\text{mut}}$  obtained using the approximate analytical expression derived in Eq. (34) to the exact mutual information  $I_{ij}$  between sites  $i$  and  $j$ , with  $l = |j - i - 1|$ . Here  $N = 12$ .

## 2. Contiguous blocks approximation

Next, let us estimate the link strengths from the EE of contiguous blocks, using expression (22), which will be denoted by  $J_r^{\text{cont}} \equiv J_{i,i+r}$ . Within this approximation, we only need to know the EE of contiguous blocks,  $S(r-1)$ ,  $S(r)$  and  $S(r+1)$ . As in the previous case, we will find that  $J_r^{\text{cont}}$  also decays exponentially with  $r$ .

We must obtain an analytical expression for the block entropies  $S(r)$ . Let us rewrite the general MPS form given in Eq. (28) as

$$|\Psi\rangle = \sum_{\alpha,\beta} |\phi_{\alpha\beta}^r\rangle |\phi_{\beta\alpha}^{N-r}\rangle, \quad (36)$$

where  $|\phi_{\alpha\beta}^r\rangle = \sum_{i_1 i_2 \dots i_r} \langle \alpha | A_{i_1} \dots A_{i_r} | \beta \rangle |i_1 \dots i_r\rangle$  and  $|\phi_{\beta\alpha}^{N-r}\rangle = \sum_{i_{r+1} i_{r+2} \dots i_N} \langle \beta | A_{i_{r+1}} \dots A_{i_N} | \alpha \rangle |i_{r+1} \dots i_N\rangle$ . Now in general the sets of basis vectors  $\{|\phi_{\alpha\beta}^r\rangle\}$  or  $\{|\phi_{\beta\alpha}^{N-r}\rangle\}$  are not orthogonal, thus forcing us to apply Gram-Schmidt's procedure to orthogonalize them in order to obtain the Schmidt decomposition,

$$|\Psi\rangle = \sum_k \frac{1}{\sqrt{\lambda_k^r \lambda_k^{N-r}}} |\psi_k^r\rangle |\psi_k^{N-r}\rangle, \quad (37)$$

where  $|\psi_k^r\rangle = \sum_{\alpha\beta} c_{\alpha\beta}^k |\phi_{\alpha\beta}^r\rangle$  and  $|\psi_k^{N-r}\rangle = \sum_{\alpha\beta} d_{\alpha\beta}^k |\phi_{\alpha\beta}^{N-r}\rangle$  with  $\langle \psi_{k'}^r | \psi_k^r \rangle = \delta_{kk'} \lambda_k^r$ ,  $\langle \psi_{k'}^{N-r} | \psi_k^{N-r} \rangle = \delta_{kk'} \lambda_k^{N-r}$  and we define  $\Lambda(r, N)_k \equiv \lambda_k^r \lambda_k^{N-r}$ . Thus the entropy for the  $r : N - r$  bipartition is given by

$$S(r) = - \sum_k \Lambda(r, N)_k \log \Lambda(r, N)_k. \quad (38)$$

Now the Schmidt values  $\lambda_k^r \lambda_k^{N-r}$  can be obtained in terms of the right and left eigenvectors of the transfer matrix (see Appendix D), and we can finally write  $\Lambda(r, N)_k$  as

$$\Lambda(r, N)_k = \lambda_k^r \lambda_k^{N-r} \equiv \Lambda_k + \sum_s \gamma_s^r \Lambda_k^s, \quad (39)$$

where we denote

$$\Lambda_k = \left( \sum_{\alpha,\beta} |c_{\alpha\beta}|^2 \langle \alpha \alpha | R_0 \rangle \langle L_0 | \beta \beta \rangle \right) \left( \sum_{\alpha,\beta} |d_{\alpha\beta}|^2 \langle \alpha \alpha | R_0 \rangle \langle L_0 | \beta \beta \rangle \right), \quad (40)$$

and  $\Lambda_k^s$  is the coefficient of  $\gamma_s^r$  appearing in the higher order terms. Plugging these in Eq. (38), we get

$$S(r) = - \sum_k \Lambda_k(r, N) \log \Lambda_k(r, N) = - \sum_k \left( \Lambda_k + \sum_s \gamma_s^r \Lambda_k^s \right) \log \left( \Lambda_k + \sum_s \gamma_s^r \Lambda_k^s \right). \quad (41)$$

Now expanding the logarithm as  $\log(\Lambda_k + \sum_s \gamma_s^r \Lambda_k^s) \approx \log(\Lambda_k) + \sum_s \gamma_s^r \frac{\Lambda_k^s}{\Lambda_k}$ , we reach

$$S(r) = S_0 - \sum_s \gamma_s^r \omega_s - \sum_{ss'} \gamma_s^r \gamma_{s'}^r \Gamma_{ss'}, \quad (42)$$

where we have denoted  $S_0 = -\Lambda_k \log \Lambda_k$ ,  $\omega_s \equiv \sum_k \Lambda_k^s (1 + \log \Lambda_k)$  and  $\Gamma_{ss'} = \sum_k \frac{\Lambda_k^s \Lambda_k^{s'}}{\Lambda_k}$ . Hence, we can see that all the block entropies  $S(r)$  converge to the thermodynamic value  $S_0$  as a power of the  $\gamma_s$ .

We are now ready to find the analytical expression of the  $J_r^{\text{cont}}$ . Plugging the expression of  $S(r)$  in Eq. (22), we finally get

$$\begin{aligned} J_r^{\text{cont}} &= S(r) - \frac{S(r-1)}{2} - \frac{S(r+1)}{2} \\ &= -\sum_s \gamma_s^r \omega_s - \sum_{ss'} \gamma_s^r \gamma_{s'}^r \Gamma_{ss'} + \frac{1}{2} \sum_s \gamma_s^{r-1} \omega_s + \frac{1}{2} \sum_{ss'} \gamma_s^{r-1} \gamma_{s'}^{r-1} \Gamma_{ss'} + \frac{1}{2} \sum_s \gamma_s^{r+1} \omega_s + \frac{1}{2} \sum_{ss'} \gamma_s^{r+1} \gamma_{s'}^{r+1} \Gamma_{ss'}, \\ &= -\sum_s \gamma_s^r \left(1 - \frac{\gamma_s}{2} - \frac{\gamma_s^{-1}}{2}\right) \omega_s - \sum_{ss'} \gamma_s^r \gamma_{s'}^r \left(1 - \frac{\gamma_s \gamma_{s'}}{2} - \frac{\gamma_s^{-1} \gamma_{s'}^{-1}}{2}\right) \Gamma_{ss'}. \end{aligned} \quad (43)$$

Hence, the link strengths  $J_r^{\text{cont}}$  decay as a power of  $\gamma_s$  and for large  $r$ , eventually decays to zero, indicating area-law feature in the quantum many-body state.

Table III compares the values of  $J_r^{\text{cont}}$  obtained through Eq. (43) to the optimal link strengths, denoted as  $J_r^{\text{opt}}$ . From the comparison we note that  $J_r^{\text{cont}}$  almost coincides with  $J_r^{\text{opt}}$  for all  $r$  and  $h_z$  values.

| $h_z$ | $r$ | $J_r^{\text{opt}}$ | $J_r^{\text{cont}}$ | $h_z$ | $r$ | $J_r^{\text{opt}}$ | $J_r^{\text{cont}}$ |
|-------|-----|--------------------|---------------------|-------|-----|--------------------|---------------------|
| 1.4   | 1   | 0.09318            | 0.09776             | 2.0   | 1   | 0.06066            | 0.05859             |
|       | 2   | 0.02318            | 0.02128             |       | 2   | 0.01006            | 0.01146             |
|       | 3   | 0.00647            | 0.00646             |       | 3   | 0.00200            | 0.00183             |
|       | 4   | 0.00216            | 0.00206             |       | 4   | 0.00042            | 0.00029             |
|       | 5   | 0.00097            | 0.00068             |       | 5   | 0.00002            | 0.00004             |

Table III: Comparison of the values of  $J_r^{\text{cont}}$  obtained using approximate analytical formula for contiguous blocks, Eq. (42) with the optimal values,  $J_r^{\text{opt}}$ , for the Ising model in a transverse field, Eq. (35), always using  $N = 12$ .

We may conclude that the link strengths for matrix product states, when they are approximated using either Eq. (34) or (43) decay exponentially with a certain correlation length associated to the second maximal eigenvalue of the transfer matrix. In fact, this property may be considered the hallmark of the area law.

## V. PHYSICAL APPLICATIONS OF THE LINK REPRESENTATION

In this section we apply the link representation formalism to the analysis of two different physical systems of interest. First of all, we will consider the different phases of a long-range spin-1/2 Hamiltonian. Then, we will consider the phase diagram of the bilinear-biquadratic spin-1 Hamiltonian.

### A. Long-range Hamiltonian

In order to explore the effect of long-range interactions on the emergent geometry, we start our numerical investigation computing the link representation for the GS of an interacting Hamiltonian presenting long-range interaction, thus generalizing results from the previous work [29], where we considered only similar systems in the short-range regime. For that purpose, we consider the long-range spin-1/2 XYZ Hamiltonian where the spin-spin couplings follow a power-law decay, which can be expressed as

$$H = \sum_{i>j} \frac{1}{|i-j|^\alpha} (t_x S_i^x S_j^x + t_y S_i^y S_j^y + t_z S_i^z S_j^z), \quad (44)$$

where  $S^k$  are the Pauli spin-1/2 operators  $\{k \in x, y, z\}$ ,  $\alpha > 0$  is the interaction exponent, and we consider periodic boundaries. The model exhibits a very rich phase diagram. In the ferromagnetic case,  $t_x = t_y = -1$ , apart from the gapless XY phase and the ferromagnetic phase that appears in the short-range limit ( $\alpha \gg 1$ ), at small values of  $\alpha$  ( $\alpha \leq 3$ ) a gapless continuous symmetry breaking (CSB) emerges [38]. In addition to this, for  $t_x = t_y = t_z$  and  $\alpha = 2$ , the model reduces to the Haldane-Shastry model, which is exactly solvable [39, 40]. Along with this, in recent times, bipartite [41] and multipartite [42] entanglement studies of the model have revealed several other interesting properties.

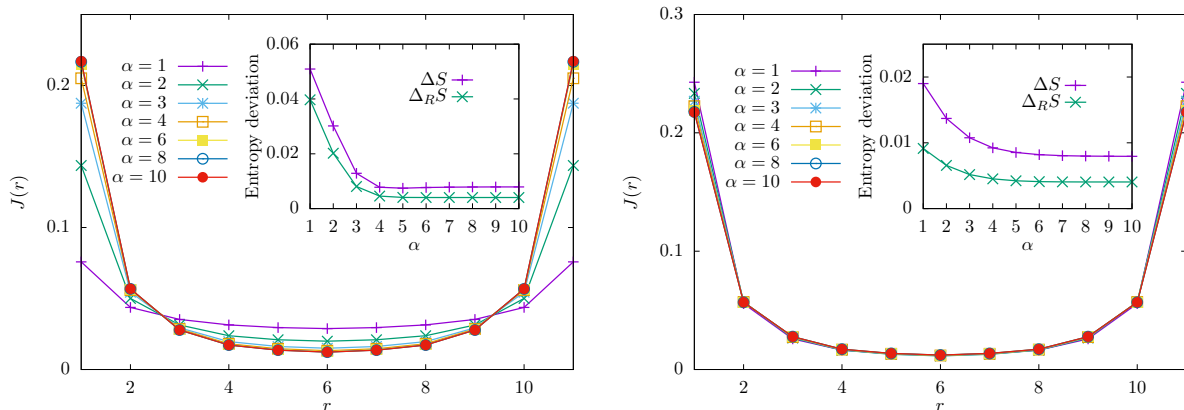


Figure 12: Left: decay of  $J(r)$  with the site distance  $r$  computed for the long-range Hamiltonian defined in Eq. (44) for different interaction exponents  $\alpha$ . Here, we consider the interaction in the XY plane to be ferromagnetic ( $t_x = t_y = -1$ ) and  $t_z = 1/2$ , for  $N = 12$ . The inset depicts the behavior of the absolute error ( $\Delta S$ ) and relative error ( $\Delta_{RS}$ ) as quantified in Eq. 10 and Eq. 11 respectively, with the long-range parameter  $\alpha$ . Right. Same plot for an antiferromagnetic interaction in the XY plane,  $t_x = t_y = 1$ .

In the following, we compute the link strengths  $J_{ij}$ , which reduce to  $J(r) = J_{i,i+r}$  due to the translational invariance, for the ferromagnetic ( $t_x = t_y = -1$ ) and antiferromagnetic ( $t_x = t_y = 1$ ) interactions in the XY plane, emphasizing the role of long-range interaction.

### 1. Ferromagnetic interaction in the XY plane: $t_x = t_y = -1$

We first consider the case when the interaction in the XY plane is ferromagnetic ( $t_x = t_y = -1$ ) and plot the behavior of  $J(r)$  with  $r$  for different values of  $\alpha$  in Fig. 12 (left). The case  $\alpha = 1$  corresponds to the long-range scenario and the case  $\alpha = 10$  to the short-range limit [29]. The profiles of  $J(r)$  show a clear dependence on the interaction exponent  $\alpha$ . In particular, for  $\alpha = 1$ ,  $J(r)$  becomes almost flat for  $r \geq 2$ , which is very different from the short-range limit. Moreover, we note that this behavior is very much akin to that obtained for the symmetry-broken antiferromagnetic phase of the model that arises in the short-range limit ( $|t_z| \gg |t_x| = |t_y|$ ,  $\alpha \gg 1$ ) which we have already explored in [29]. Such a dependence of  $J(r)$  on the interaction exponent remains significant up to  $\alpha \leq 3$ , i.e. while the system remains in the CSB phase. Beyond that point, the plots for different values of  $\alpha$  correspond to the short range limit. Additionally, we note that both absolute ( $\Delta S$ ) and relative ( $\Delta_{RS}$ ) errors of the entropies are maximum for the perfect long-range case ( $\alpha = 1$ ) and decays with  $\alpha$ .

### 2. Antiferromagnetic interaction in XY plane: $t_x = t_y = 1$

We next consider the case when the interaction in the XY plane is antiferromagnetic, i.e.,  $t_x = t_y = 1$ . The behavior of  $J(r)$  for different interaction exponents is shown in Fig. 12 (right). From the figure, we can see that unlike the ferromagnetic case, the  $J(r)$  profiles present a very mild dependence on  $\alpha$ , and  $J(r)$  always decays fast. In



the short-range limit, the ferromagnetic model becomes almost indistinguishable from the antiferromagnetic one and that is reflected in the identical profiles of  $J(r)$  for  $\alpha \approx 10$ . In this case, we also note that in the long-range limit, both absolute error ( $\Delta S$ ) and relative error ( $\Delta_R S$ ) obtained remain relatively smaller than the ferromagnetic case.

From these two cases we are led to claim that the GS of Hamiltonian (44) presents a 1D entanglement geometry for the ferromagnetic case with  $\alpha \geq 3$  and the anti-ferromagnetic case for all values of the interaction exponent. Notice that the error of the link representation is always lower when the entanglement geometry is well defined. Indeed, the error associated to the optimal link representation can be considered as a measure of *departure* from a generalized version of the area law.

## B. Spin-1 Bilinear-Biquadratic Hamiltonian

We next extend our investigation to a higher spin system, the spin-1 bilinear-biquadratic Heisenberg (BBH) chain with periodic boundaries [43–45], which can be expressed as

$$H_{BBH} = \sum_i^N \cos(\theta) \vec{S}_i \cdot \vec{S}_{i+1} + \sin(\theta) \left( \vec{S}_i \cdot \vec{S}_{i+1} \right)^2, \quad (45)$$

where  $\vec{S}_i$  are the spin-1 operators. In our case, we mainly focus on the Haldane phase of the model [46], which appears in the range  $-\frac{\pi}{4} < \theta < \frac{\pi}{4}$ . The GS obtained in this region is unique and separated by a finite gap from the first excited state. We obtain the ground state of the model which is a singlet, using exact diagonalization for different values of  $\theta$  and compute the corresponding link matrices from the distribution of the entanglement in all its possible bipartitions.

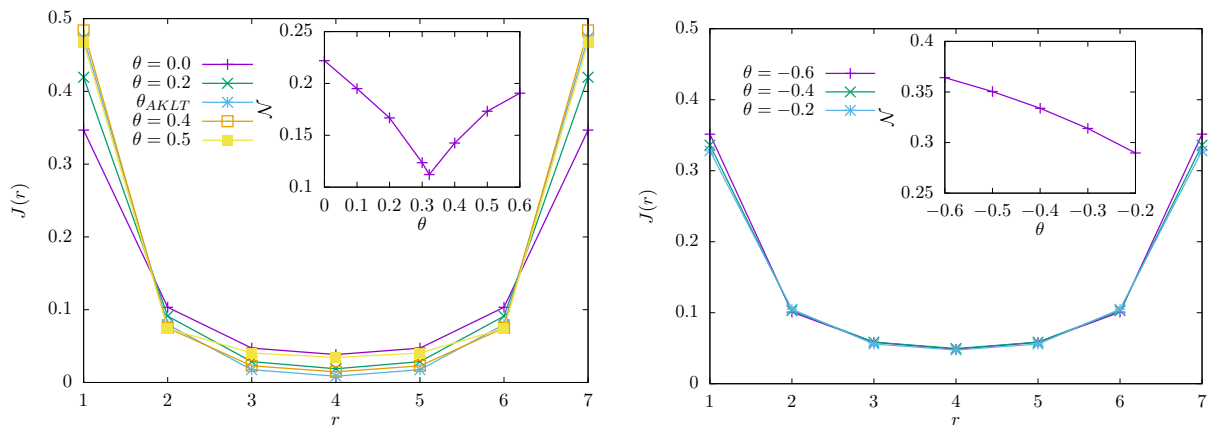


Figure 13: Left: Plot of  $J(r)$  for the GS of the BBH Hamiltonian defined in Eq. (45) for different values of  $\theta$ . The profile obtained at the AKLT point ( $\theta = \arctan(\frac{1}{3})$ ) yields the minimum value of  $J(r)$  for  $r \geq 2$ . In the inset, we plot the behavior of the negativity ( $\mathcal{N}$ ) obtained for reduced density matrix  $\rho_{ij}$  of any two nearest-neighbor sites  $i, j$  with  $\theta$ . In all cases,  $N = 8$ . Right: Same plot for negative values of  $\theta$ .

### 1. $\theta \geq 0$ region

We first consider the positive  $\theta$  region of the Haldane phase and obtain the behavior of the link strengths,  $J(r)$ . The profiles obtained for different  $\theta$  values are shown in Fig. 13 (left). From the figure, one can observe that there is a clear dependence of  $J(r)$  on  $\theta$ . For  $r = 1$ , the link strength  $J(r)$  increases with  $\theta$ , while for  $r \geq 2$ , it exhibits the opposite behavior and for any fixed value of  $r$  ( $2 \leq r \leq N/2$ ), the value of  $J(r)$  obtained for  $\theta = \theta_{AKLT} = \arctan(\frac{1}{3})$  turns out to be minimum. The reason is that AKLT is actually the fixed point of a real space renormalization group, so one expects that all entanglement will be concentrated in the nearest neighbour sites.

This behavior is consistent with the entanglement properties explored in this region. For example, it is known that the entanglement negativity, defined as

$$\mathcal{N}(\rho) = \frac{|\rho_{ij}|^{T_j} - 1}{2}, \quad (46)$$

where  $T_j$  is the partial transpose of the reduced system  $\rho_{ij}$  with respect to subsystem  $j$  and  $|\cdot|$  is the trace norm, exhibits a local minimum at the AKLT point [45], shown at the inset of Fig. 13 (left).

## 2. $\theta < 0$ region

The behavior of link representation obtained for the  $\theta < 0$  region of the Haldane phase is very different from that obtained for  $\theta \geq 0$ . We found that in this region, the link strengths  $J(r)$  present a very mild dependence on  $\theta$  only for  $r = 1$  and become independent of  $\theta$  from  $r \geq 2$ . Hence, all the  $J(r)$  profiles seem to collapse, as shown in Fig. 13 (right). Similarly to the positive  $\theta$  region, this behavior is also found to be consistent with the behavior of entanglement in this region [45]. In particular, the negativity,  $\mathcal{N}$ , obtained for two neighboring sites shows a slow decay with  $\theta$ . For completeness, we also plot the behavior of  $\mathcal{N}$  with  $\theta$  in the inset of Fig. 13 (right).

Fig. 14 shows the absolute ( $\Delta S$ ) and relative ( $\Delta_{RS}$ ) error, as defined in Eq. (10) and Eq. (11) respectively, for the link representation of the GS of the BBH Hamiltonian as a function of  $\theta$ . We can observe that the error remains relatively low,  $\Delta S \sim 0.02$ ,  $\Delta_{RS} \sim 0.01$  for  $\theta < 0.2$ , and grows substantially above that point.

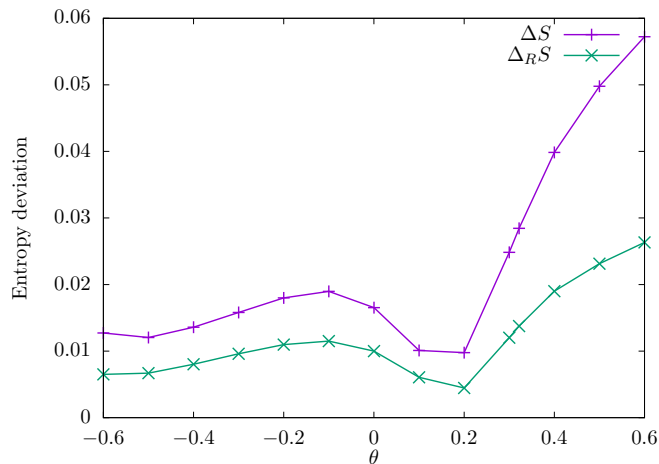


Figure 14: Error analysis for BBH Hamiltonian as defined in Eq. (45). We compare both absolute ( $\Delta S$ ) and relative ( $\Delta_{RS}$ ) error for different values of  $\theta$ . Here  $N=8$ .

## VI. CONCLUSIONS AND FURTHER WORK

The entanglement entropies of all possible bipartitions of a pure state of a quantum system can be expressed in a simple form via the *link representation*, Eq. (1), i.e. the entropy of any block can be estimated summing the *link strengths* between sites of the block and sites of the environment. In [29] a procedure to obtain the optimal link representation of a given quantum state was presented, along with a proof that the most relevant properties of entanglement (e.g. strong subadditivity) were naturally fulfilled.

In this article we provide an analysis of the accuracy of the link representation for different types of states, focusing on a conformally invariant free-fermionic state and on random states. The accuracy of the link representation is very high for the conformally invariant state, and increases with the system size. For the random state, on the other hand, we observe that the accuracy is much worse, showing that the link representation is valuable when the system presents some effective area law, even if logarithmic corrections are required.

The high computational cost of obtaining the optimal link representation suggests the search of effective approximate methods. We provide several which provide a very good accuracy. Instead of considering the entanglement entropies for all bipartitions we may restrict ourselves to a random sample, and we show that a number of samples corresponding

to a few times the number of parameters is enough for a good accuracy. Moreover, we provide an approximate link representation based on the knowledge of compact blocks, and another one specially suited for free-fermionic states.

We have also considered the link representation of matrix product states (MPS). We have shown that the link strengths for an MPS decay exponentially with the distance, with the correlation length corresponding to the inverse of the second highest eigenvalue of the transfer matrix. In order to prove that result, we have computed the mutual information of pairs of sites and the entropy of contiguous blocks in generic MPS, and applied them to the evaluation of the link strengths for the off-critical Ising model in a transverse field.

We have obtained the link representation of the GS of two relevant physical models, in order to check how the accuracy and the link strengths signal the presence of different quantum phases. For the Heisenberg model with long-range interactions, we have found that the accuracy of the link representation becomes higher in the short-range phase, which shows that this accuracy can be used to signal departure from the area law. The behavior of the link strengths is also different in the long-range phase, becoming homogeneous, as they do for random states. Also, we have considered the spin-1 bilinear-biquadratic Hamiltonian in the vicinity of the AKLT point, showing that the representation of the entanglement entropies of the state is good, as they should because the states can be represented as MPS of low bond dimension.

### Acknowledgments

We would like to thank P. Calabrese, J.I. Cirac, J.I. Latorre, E. López, L. Tagliacozzo, E. Tonni, G. Vidal, H.Q. Zhou, Q.Q. Shi and S.Y. Cho for conversations. We acknowledge financial support from the grants PGC2018-095862-B-C21, PGC2018-094763-B-I00, PID2019-105182GB-I00, QUITEMAD+ S2013/ICE-2801, SEV-2016-0597 of the *Centro de Excelencia Severo Ochoa* Programme and the CSIC Research Platform on Quantum Technologies PTI-001.

### Appendix A: Graphical proof of $(\Delta_2\Delta_1S)_{i,j} = 2J_{i,j}$

In this section we present a graphical proof of Eq. (20) from the main text. The black plus signs correspond to the entanglement links which we must add to obtain  $S_{i,j}$ , while the red plus signs and the green and blue minus signs correspond to the other terms in the equation. Indeed, we can easily check that all plus and minus signs cancel out except for the element  $(i, j)$ , which contains two plus signs, as claimed in Eq. (20).

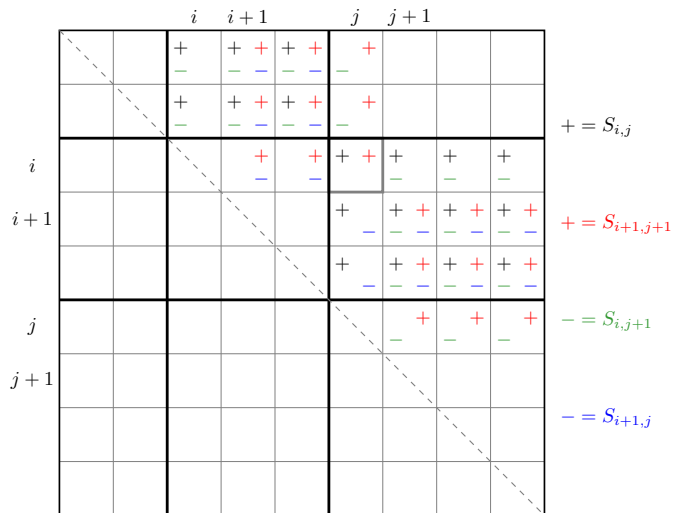


Figure 15: Graphical proof of Eq. (20). We show the full  $J$ -matrix, highlighting the the entanglement links contributing to  $S_{i,j}$  (black, +),  $S_{i+1,j+1}$  (red, +),  $S_{i+1,j}$  (blue -) and  $S_{i,j+1}$  (green, -). Notice that all entanglement links cancel out except  $J_{i,j}$ , which gets two positive signs.

### Appendix B: Few-sites reduced density matrix for MPS

We start with a matrix product state representation as given in Eq. (28) in the main text

$$|\Psi\rangle = \sum_{i_1 i_2 \dots i_N} \text{Tr}(A_{i_1} A_{i_2} \dots A_{i_N}) |i_1 i_2 \dots i_N\rangle. \quad (\text{B1})$$

Now consider the reduced density matrix  $\rho_{ij}$ , which can be obtained from  $|\psi\rangle$  by tracing out all but the sites  $i$  and  $j$ , as follows

$$\rho_{ij} = \text{Tr}_{\overline{\{i,j\}}} |\Psi\rangle\langle\Psi|. \quad (\text{B2})$$

Now from the schematic in Fig. 11 of the main text, it is easy to realize

$$\rho_{ij} = \text{Tr}(E^{l_L} \bar{E}_i E^l \bar{E}_j E^{l_R}), \quad (\text{B3})$$

where we consider the system is translational invariant and  $\bar{E}_k = \sum_{k_m k_n} (A_{k_m} \otimes A_{k_n}^*) |k_m\rangle\langle k_n|$ . Expanding  $E = |R_0\rangle\langle L_0| + \sum_s \gamma_s |R_s\rangle\langle L_s|$ , we get

$$\begin{aligned}
\rho_{ij} &= \text{Tr} \left[ \left( |R_0\rangle\langle L_0| + \sum_q \gamma_q^{l_L} |R_q\rangle\langle L_q| \right) \bar{E}_i (|R_0\rangle\langle L_0| + \gamma_1^l |R_1\rangle\langle L_1|) \bar{E}_j \left( |R_0\rangle\langle L_0| + \sum_p \gamma_p^{l_R} |R_p\rangle\langle L_p| \right) \right], \\
&= \text{Tr} (|R_0\rangle\langle L_0| \bar{E}_i |R_0\rangle\langle L_0| \bar{E}_j |R_0\rangle\langle L_0|) + \text{Tr} (\gamma_1^l |R_0\rangle\langle L_0| \bar{E}_i |R_1\rangle\langle L_1| \bar{E}_j |R_0\rangle\langle L_0|) \\
&+ \text{Tr} \left( \sum_{pq} \gamma_q^{l_L} \gamma_p^{l_R} |R_q\rangle\langle L_q| \bar{E}_i |R_0\rangle\langle L_0| \bar{E}_j |R_p\rangle\langle L_p| \right) + \text{Tr} \left( \sum_{pq} \gamma_q^{l_L} \gamma_p^{l_R} \gamma_s^l |R_q\rangle\langle L_q| \bar{E}_i |R_1\rangle\langle L_1| \bar{E}_j |R_p\rangle\langle L_p| \right), \\
&= \langle L_0 | \bar{E}_i | R_0 \rangle \langle L_0 | \bar{E}_j | R_0 \rangle + \gamma_1^l \langle L_0 | \bar{E}_i | R_1 \rangle \langle L_1 | \bar{E}_j | R_0 \rangle + \sum_{pq} \delta_{pq} \gamma_q^{l_L} \gamma_p^{l_R} \langle L_q | \bar{E}_i | R_0 \rangle \langle L_0 | \bar{E}_j | R_p \rangle \\
&+ \sum_{pq} \delta_{pq} \gamma_q^{l_L} \gamma_p^{l_R} \gamma_s^l \langle L_q | \bar{E}_i | R_1 \rangle \langle L_1 | \bar{E}_j | R_p \rangle, \\
&= \langle L_0 | \bar{E}_i | R_0 \rangle \langle L_0 | \bar{E}_j | R_0 \rangle + \gamma_1^l \langle L_0 | \bar{E}_i | R_1 \rangle \langle L_1 | \bar{E}_j | R_0 \rangle + \sum_q \gamma_q^{l_L + l_R} \langle L_q | \bar{E}_i | R_0 \rangle \langle L_0 | \bar{E}_j | R_q \rangle \\
&+ \sum_{qs} \gamma_q^{l_L + l_R} \gamma_s^l \langle L_q | \bar{E}_i | R_s \rangle \langle L_s | \bar{E}_j | R_q \rangle.
\end{aligned} \tag{B4}$$

Using  $l_L + l_R \gg 1$ , we get

$$\begin{aligned}
\rho_{ij} &= \sum_{i_m i_n j_m j_n} \langle L_0 | A_{i_m} \otimes A_{i_n}^* | R_0 \rangle \langle L_0 | A_{j_m} \otimes A_{j_n}^* | R_0 \rangle |i_m j_m\rangle \langle i_n j_n| \\
&+ \gamma_1^l \sum_{i_m i_n j_m j_n} \langle L_0 | A_{i_m} \otimes A_{i_n}^* | R_1 \rangle \langle L_1 | A_{j_m} \otimes A_{j_n}^* | R_0 \rangle |i_m j_m\rangle \langle i_n j_n|, \\
&= \rho_i \otimes \rho_j + \gamma_1^l \tilde{\rho}_{ij},
\end{aligned} \tag{B5}$$

with  $\rho_i \otimes \rho_j = \sum_{i_m i_n j_m j_n} \langle L_0 | A_{i_m} \otimes A_{i_n}^* | R_0 \rangle \langle L_0 | A_{j_m} \otimes A_{j_n}^* | R_0 \rangle |i_m j_m\rangle \langle i_n j_n|$ , and  $\tilde{\rho}_{ij} = \sum_{i_m i_n j_m j_n} \langle L_0 | A_{i_m} \otimes A_{i_n}^* | R_1 \rangle \langle L_1 | A_{j_m} \otimes A_{j_n}^* | R_0 \rangle |i_m j_m\rangle \langle i_n j_n|$ .

### Appendix C: Mutual information between sites for MPS

We start with the expansion of the logarithm

$$\log(\rho_{ij}) = \log(\rho_{ij}^0 + \gamma_1^l \tilde{\rho}_{ij}) = \log(\rho_{ij}^0) + \gamma_1^l \int_0^\infty \frac{1}{\rho_{ij}^0 + z} \tilde{\rho}_{ij} \frac{1}{\rho_{ij}^0 + z} dz - \gamma_1^{2l} \int_0^\infty \frac{1}{\rho_{ij}^0 + z} \tilde{\rho}_{ij} \frac{1}{\rho_{ij}^0 + z} \tilde{\rho}_{ij} \frac{1}{\rho_{ij}^0 + z} dz + O(\gamma_1^{2l+1}). \tag{C1}$$

Hence,

$$\begin{aligned}
-\rho_{ij} \log(\rho_{ij}) &= -(\rho_{ij}^0 + \gamma_1^l \tilde{\rho}_{ij}) \log(\rho_{ij}^0 + \gamma_1^l \tilde{\rho}_{ij}), \\
&= -(\rho_{ij}^0 + \gamma_1^l \tilde{\rho}_{ij}) \log(\rho_{ij}^0) - \gamma_1^l (\rho_{ij}^0 + \gamma_1^l \tilde{\rho}_{ij}) \int_0^\infty \frac{1}{\rho_{ij}^0 + z} \tilde{\rho}_{ij} \frac{1}{\rho_{ij}^0 + z} dz, \\
&+ \gamma_1^{2l} (\rho_{ij}^0 + \gamma_1^l \tilde{\rho}_{ij}) \int_0^\infty \frac{1}{\rho_{ij}^0 + z} \tilde{\rho}_{ij} \frac{1}{\rho_{ij}^0 + z} \tilde{\rho}_{ij} \frac{1}{\rho_{ij}^0 + z} dz + O(\gamma_1^{2l+1}), \\
&= -\rho_{ij}^0 \log(\rho_{ij}^0) - \gamma_1^l \left[ \tilde{\rho}_{ij} \log(\rho_{ij}^0) + \rho_{ij}^0 \int_0^\infty \frac{1}{(\rho_{ij}^0 + z)} \tilde{\rho}_{ij} \frac{1}{(\rho_{ij}^0 + z)} dz \right] \\
&- \gamma_1^{2l} \left[ \tilde{\rho}_{ij} \int_0^\infty \frac{1}{(\rho_{ij}^0 + z)} \tilde{\rho}_{ij} \frac{1}{(\rho_{ij}^0 + z)} dz - \rho_{ij}^0 \int_0^\infty \frac{1}{(\rho_{ij}^0 + z)} \tilde{\rho}_{ij} \frac{1}{(\rho_{ij}^0 + z)} \tilde{\rho}_{ij} \frac{1}{(\rho_{ij}^0 + z)} dz \right] + O(\gamma_1^{2l+1}).
\end{aligned} \tag{C2}$$

Let us now consider the terms in the integral.

$$S(\rho_{ij}) = S(\rho_{ij}^0) - \gamma_1^l \left[ \text{Tr}(\bar{\rho}_{ij} \log \rho_{ij}^0) + \text{Tr} \left( \rho_{ij}^0 \int_0^\infty \frac{1}{\rho_{ij}^0 + z} \bar{\rho}_{ij} \frac{1}{\rho_{ij}^0 + z} dz \right) \right] - \gamma_1^{2l} \left[ \text{Tr} \left( \bar{\rho}_{ij} \int_0^\infty \frac{1}{\rho_{ij}^0 + z} \bar{\rho}_{ij} \frac{1}{\rho_{ij}^0 + z} dz \right) \right. \\ \left. - \text{Tr} \left( \rho_{ij}^0 \int_0^\infty \frac{1}{\rho_{ij}^0 + z} \bar{\rho}_{ij} \frac{1}{\rho_{ij}^0 + z} \bar{\rho}_{ij} \frac{1}{\rho_{ij}^0 + z} dz \right) \right]. \quad (\text{C3})$$

**1. First term:**  $\text{Tr} \left( \rho_{ij}^0 \int_0^\infty \frac{1}{\rho_{ij}^0 + z} \bar{\rho}_{ij} \frac{1}{\rho_{ij}^0 + z} dz \right)$ : Consider  $\rho_{ij}^0$  has eigenvalues  $E_m$ . Hence, the eigenvalue of  $(\rho_{ij}^0 + z)^{-1}$  is given by  $(E_m + z)^{-1}$ . Now, if we express everything in the basis of  $\rho_{ij}^0$ , we would get

$$\rho_{ij}^0 \frac{1}{\rho_{ij}^0 + z} \bar{\rho}_{ij} \frac{1}{\rho_{ij}^0 + z} = \sum_m E_m (E_m + z)^{-2} \bar{\rho}_{ij}(mm), \quad (\text{C4})$$

where  $\bar{\rho}_{ij}$  is  $\bar{\rho}_{ij}$ , expressed in the eigebasis of  $\rho_{ij}^0$  and  $E_m$  are eigenvalues of  $\rho_0$ . If we integrate C4, we would get

$$\int_0^\infty \sum_m E_m (E_m + z)^{-2} \bar{\rho}_{ij}(mm) dz = \sum_m E_m \bar{\rho}_{ij}(mm) \int_0^\infty (E_m + z)^{-2} dz, \\ = - \sum_m E_m \left[ \frac{1}{E_m + z} \right]_0^\infty \bar{\rho}_{ij}(mm) = \sum_m \bar{\rho}_{ij}(mm) = 0. \quad (\text{C5})$$

Hence, we finally get  $\text{Tr} \left( \rho_{ij}^0 \int_0^\infty \frac{1}{\rho_{ij}^0 + z} \bar{\rho}_{ij} \frac{1}{\rho_{ij}^0 + z} dz \right) = 0$ .

**2. Second term:**  $\text{Tr} \left( \bar{\rho}_{ij} \int_0^\infty \frac{1}{\rho_{ij}^0 + z} \bar{\rho}_{ij} \frac{1}{\rho_{ij}^0 + z} dz \right)$ : We can again proceed as before and show that

$$\text{Tr} \left( \bar{\rho}_{ij} \frac{1}{\rho_{ij}^0 + z} \bar{\rho}_{ij} \frac{1}{\rho_{ij}^0 + z} \right) = \sum_{mn} \bar{\rho}_{ij}(mn) \bar{\rho}_{ij}(nm) (E_m + z)^{-1} (E_n + z)^{-1}. \quad (\text{C6})$$

We will integrate the above term later.

**3. Third term:**  $-\text{Tr} \left( \rho_{ij}^0 \int_0^\infty \frac{1}{\rho_{ij}^0 + z} \bar{\rho}_{ij} \frac{1}{\rho_{ij}^0 + z} \bar{\rho}_{ij} \frac{1}{\rho_{ij}^0 + z} dz \right)$ .

This term is very similar to previous one, except, we have here additional factor  $\rho_{ij}^0 \frac{1}{\rho_{ij}^0 + z}$ , which is diagonal in the basis of  $\rho_{ij}^0$ , and when multiplied with rest of the term  $\bar{\rho}_{ij} \frac{1}{\rho_{ij}^0 + z} \bar{\rho}_{ij} \frac{1}{\rho_{ij}^0 + z}$  just contributes  $E_m (E_m + z)^{-1}$  in the diagonal.

Hence, if we sum second and third term. we would get

$$\text{Tr} \left( \bar{\rho}_{ij} \frac{1}{\rho_{ij}^0 + z} \bar{\rho}_{ij} \frac{1}{\rho_{ij}^0 + z} \right) - \text{Tr} \left( \rho_{ij}^0 \frac{1}{\rho_{ij}^0 + z} \bar{\rho}_{ij} \frac{1}{\rho_{ij}^0 + z} \bar{\rho}_{ij} \frac{1}{\rho_{ij}^0 + z} \right), \\ = \sum_{mn} \bar{\rho}_{ij}(mn) \bar{\rho}_{ij}(nm) (E_m + z)^{-1} (E_n + z)^{-1} (1 - E_m (E_m + z)^{-1}), \\ = \sum_{mn} \bar{\rho}_{ij}(mn) \bar{\rho}_{ij}(nm) z (E_m + z)^{-2} (E_n + z)^{-1}. \quad (\text{C7})$$

We will now integrate the above term,

$$\text{Tr} \left( \bar{\rho}_{ij} \int_0^\infty \frac{1}{\rho_{ij}^0 + z} \bar{\rho}_{ij} \frac{1}{\rho_{ij}^0 + z} dz \right) - \text{Tr} \left( \rho_{ij}^0 \int_0^\infty \frac{1}{\rho_{ij}^0 + z} \bar{\rho}_{ij} \frac{1}{\rho_{ij}^0 + z} \bar{\rho}_{ij} \frac{1}{\rho_{ij}^0 + z} dz \right) \\ = \sum_{mn} \bar{\rho}_{ij}(mn) \bar{\rho}_{ij}(nm) \int_0^\infty z (E_m + z)^{-2} (E_n + z)^{-1} dz. \quad (\text{C8})$$

Now for  $m \neq n$ , let us write  $z(E_m + z)^{-2}(E_n + z)^{-1} = \frac{E_m}{E_m - E_n} \frac{1}{(E_m + z)^2} + \frac{E_n}{(E_m - E_n)^2} \frac{1}{E_m + z} - \frac{E_n}{(E_m - E_n)^2} \frac{1}{E_n + z}$ . Hence, integrating, we get

$$\begin{aligned} \int_0^\infty z(E_m + z)^{-2}(E_n + z)^{-1} &= \int_0^\infty \frac{E_m}{E_m - E_n} \frac{dz}{(E_m + z)^2} + \frac{E_n}{(E_m - E_n)^2} \frac{dz}{E_m + z} - \frac{E_n}{(E_m - E_n)^2} \frac{dz}{E_n + z}, \\ &= -\frac{E_m}{E_m - E_n} \left[ \frac{1}{E_m + z} \right]_0^\infty + \frac{E_n}{(E_m - E_n)^2} \left[ \log \left( \frac{E_m + z}{E_n + z} \right) \right]_0^\infty, \\ &= \frac{1}{E_m - E_n} + \frac{E_n}{(E_m - E_n)^2} \log \left( \frac{E_n}{E_m} \right). \end{aligned} \quad (C9)$$

Similarly, for  $m = n$ , we have

$$\int_0^\infty z(E_m + z)^{-3} dz = \int_0^\infty \frac{dz}{(E_m + z)^2} - \int_0^\infty \frac{E_m}{(E_m + z)^3} dz = \left[ -\frac{1}{E_m + z} + \frac{E_m}{2(E_m + z)^2} \right]_0^\infty = \frac{1}{2E_m}. \quad (C10)$$

Combining Eqs. (C9) and (C10), we finally get

$$\begin{aligned} &\text{Tr} \left( \bar{\rho}_{ij} \int_0^\infty \frac{1}{\rho_{ij}^0 + z} \bar{\rho}_{ij} \frac{1}{\rho_{ij}^0 + z} dz \right) - \text{Tr} \left( \rho_{ij}^0 \int_0^\infty \frac{1}{\rho_{ij}^0 + z} \bar{\rho}_{ij} \frac{1}{\rho_{ij}^0 + z} \bar{\rho}_{ij} \frac{1}{\rho_{ij}^0 + z} dz \right) \\ &= \sum_m \frac{1}{2E_m} |\bar{\rho}_{ij}(mm)|^2 + \sum_{m \neq n} \left[ \frac{1}{E_m - E_n} + \frac{E_n}{(E_m - E_n)^2} \log \left( \frac{E_n}{E_m} \right) \right] |\bar{\rho}_{ij}(mn)|^2. \end{aligned} \quad (C11)$$

Now  $|\bar{\rho}_{ij}^2|$  remains unchanged under the exchange of indices  $m$  and  $n$  but  $\frac{1}{E_m - E_n}$  acquires a minus sign. Hence,  $\sum_{m,n} \frac{1}{E_m - E_n} |\bar{\rho}_{ij}(mn)|^2 = 0$ . Therefore, we can finally write

$$S(\rho) = S(\rho_0) - \gamma_1^l \text{Tr} (\bar{\rho}_{ij} \log(\rho_{ij}^0)) - \gamma_1^{2l} \left( \sum_m \frac{|\bar{\rho}_{ij}(mm)|^2}{2E_m} + \sum_{m \neq n} \left[ \frac{E_n}{(E_m - E_n)^2} \log \left( \frac{E_n}{E_m} \right) \right] |\bar{\rho}_{ij}(mn)|^2 \right). \quad (C12)$$

$$J_{ij}^{\text{mut}} = \frac{1}{2} (S(\rho_{ij}^0) - S(\rho_{ij})) = \frac{\gamma_1^l}{2} \text{Tr} (\bar{\rho}_{ij} \log(\rho_{ij}^0)) + \frac{\gamma_1^{2l}}{2} \left( \sum_m \frac{|\bar{\rho}_{ij}(mm)|^2}{2E_m} + \sum_{m \neq n} \left[ \frac{E_n}{(E_m - E_n)^2} \log \left( \frac{E_n}{E_m} \right) \right] |\bar{\rho}_{ij}(mn)|^2 \right). \quad (C13)$$

#### Appendix D: Schmidt values for MPS

From the expression of  $|\psi_k^r\rangle = \sum_{\alpha\beta} c_{\alpha\beta} |\phi_{\alpha\beta}^r\rangle$  and  $|\psi_k^{N-r}\rangle = \sum_{\alpha\beta} d_{\alpha\beta} |\phi_{\alpha\beta}^{N-r}\rangle$ , with  $|\phi_{\alpha\beta}^r\rangle = \sum_{i_1 i_2 \dots i_r} \langle \alpha | A_{i_1} \dots A_{i_r} | \beta \rangle |i_1 \dots i_r\rangle$  and  $|\phi_{\alpha\beta}^{N-r}\rangle = \sum_{i_{r+1} i_{r+2} \dots i_N} \langle \beta | A_{i_{r+1}} \dots A_{i_N} | \alpha \rangle |i_{r+1} \dots i_N\rangle$  we can obtain the Schmidt value as follows

$$\begin{aligned} \lambda_k^r = \langle \psi_k^r | \psi_k^r \rangle &= \sum_{\alpha\alpha'\beta\beta'} c_{\alpha\beta} c_{\alpha'\beta'}^* \langle \phi_{\alpha'\beta'}^r | \phi_{\alpha\beta}^r \rangle, \\ &= \sum_{\alpha=\alpha', \beta=\beta'} |c_{\alpha\beta}|^2 \langle \phi_{\alpha\beta}^r | \phi_{\alpha\beta}^r \rangle + \sum_{\alpha \neq \alpha', \beta = \beta'} c_{\alpha\beta} c_{\alpha'\beta'}^* \langle \phi_{\alpha'\beta'}^r | \phi_{\alpha\beta}^r \rangle \\ &+ \sum_{\alpha = \alpha', \beta \neq \beta'} c_{\alpha\beta} c_{\alpha'\beta'}^* \langle \phi_{\alpha'\beta'}^r | \phi_{\alpha\beta}^r \rangle + \sum_{\alpha \neq \alpha', \beta \neq \beta'} c_{\alpha\beta} c_{\alpha'\beta'}^* \langle \phi_{\alpha'\beta'}^r | \phi_{\alpha\beta}^r \rangle. \end{aligned} \quad (D1)$$

Now, using the form of  $|\phi_{\alpha\beta}^r\rangle$ , and exploiting the canonical relation one can show that

$$\langle \phi_{\alpha'\beta'}^r | \phi_{\alpha\beta}^r \rangle = \langle \alpha' | \alpha \rangle \langle R_0 | \langle L_0 | \beta' \beta \rangle \delta_{\alpha'\alpha} \delta_{\beta'\beta} + \sum_s \gamma_s^r \langle \alpha' | \alpha \rangle \langle R_s | \langle L_s | \beta' \beta \rangle. \quad (D2)$$

Similarly, for  $|\phi_{\alpha\beta}^{N-r}\rangle$ , we can write

$$\langle\phi_{\beta'\alpha'}^{N-r}|\phi_{\beta\alpha}^{N-r}\rangle = \langle\beta'\beta|R_0\rangle\langle L_0|\alpha'\alpha\rangle\delta_{\beta'\beta}\delta_{\alpha'\alpha} + \sum_s \gamma_s^{N-r} \langle\beta'\beta|R_s\rangle\langle L_s|\alpha'\alpha\rangle. \quad (\text{D3})$$

Plugging these in Eq. (D1), we get

$$\begin{aligned} \lambda_k^r &= \sum_{\alpha,\beta} |c_{\alpha\beta}|^2 \langle\alpha\alpha|R_0\rangle\langle L_0|\beta\beta\rangle + \sum_s \gamma_s^r \sum_{\alpha,\beta} |c_{\alpha\beta}|^2 \langle\alpha\alpha|R_s\rangle\langle L_s|\beta\beta\rangle \\ &+ \sum_{ss'} \gamma_s^r \sum_{\alpha\neq\alpha',\beta} c_{\alpha\beta} c_{\alpha'\beta}^* \langle\alpha'\alpha|R_s\rangle\langle L_s|\beta\beta\rangle \\ &+ \sum_{ss'} \gamma_s^r \sum_{\alpha',\beta\neq\beta'} c_{\alpha\beta} c_{\alpha'\beta'}^* \langle\alpha\alpha|R_s\rangle\langle L_s|\beta'\beta\rangle + \sum_{ss'} \gamma_s^r \sum_{\alpha\neq\alpha',\beta\neq\beta'} c_{\alpha\beta} c_{\alpha'\beta'}^* \langle\alpha'\alpha|R_s\rangle\langle L_s|\beta'\beta\rangle. \end{aligned} \quad (\text{D4})$$

Similarly,

$$\begin{aligned} \Lambda(r, N)_k &= \sum_{\alpha,\beta} |d_{\alpha\beta}|^2 \langle\alpha\alpha|R_0\rangle\langle L_0|\beta\beta\rangle + \sum_s \gamma_s^{N-r} \sum_{\alpha,\beta} |d_{\alpha\beta}|^2 \langle\alpha\alpha|R_s\rangle\langle L_s|\beta\beta\rangle \\ &+ \sum_{ss'} \gamma_s^{N-r} \sum_{\alpha\neq\alpha',\beta} d_{\alpha\beta} d_{\alpha'\beta}^* \langle\alpha'\alpha|R_s\rangle\langle L_s|\beta\beta\rangle \\ &+ \sum_{ss'} \gamma_s^{N-r} \sum_{\alpha,\beta\neq\beta'} d_{\alpha\beta} d_{\alpha'\beta'}^* \langle\alpha\alpha|R_s\rangle\langle L_s|\beta'\beta\rangle + \sum_{ss'} \gamma_s^{N-r} \sum_{\alpha\neq\alpha',\beta\neq\beta'} d_{\alpha\beta} d_{\alpha'\beta'}^* \langle\alpha'\alpha|R_s\rangle\langle L_s|\beta'\beta\rangle. \end{aligned} \quad (\text{D5})$$

Now if we consider  $N \gg 1$ , we can drop the higher order term and approximate  $\lambda_k^{N-r}$  as

$$\lambda_k^{N-r} = \sum_{\alpha,\beta} |d_{\alpha\beta}|^2 \langle\alpha\alpha|R_0\rangle\langle L_0|\beta\beta\rangle. \quad (\text{D6})$$

Hence, we can write

$$\begin{aligned} \lambda_k^N &= \lambda_k^r \lambda_k^{N-r} = \left( \sum_{\alpha,\beta} |c_{\alpha\beta}|^2 \langle\alpha\alpha|R_0\rangle\langle L_0|\beta\beta\rangle \right) \left( \sum_{\alpha,\beta} |d_{\alpha\beta}|^2 \langle\alpha\alpha|R_0\rangle\langle L_0|\beta\beta\rangle \right) \\ &+ \sum_s \gamma_s^r \left( \sum_{\alpha,\beta} |c_{\alpha\beta}|^2 \langle\alpha\alpha|R_s\rangle\langle L_s|\beta\beta\rangle \right) + \sum_{\alpha\neq\alpha',\beta} c_{\alpha\beta} c_{\alpha'\beta}^* \langle\alpha'\alpha|R_s\rangle\langle L_s|\beta\beta\rangle \\ &+ \sum_{\alpha,\beta\neq\beta'} c_{\alpha\beta} c_{\alpha'\beta'}^* \langle\alpha\alpha|R_s\rangle\langle L_s|\beta'\beta\rangle + \sum_{\alpha\neq\alpha',\beta\neq\beta'} c_{\alpha\beta} c_{\alpha'\beta'}^* \langle\alpha'\alpha|R_s\rangle\langle L_s|\beta'\beta\rangle \left( \sum_{\alpha=\alpha',\beta=\beta'} |d_{\alpha\beta}|^2 \langle\alpha\alpha|R_0\rangle\langle L_0|\beta\beta\rangle \right), \\ &= \Lambda_k + \sum_s \gamma_s^r \Lambda_k^s, \end{aligned} \quad (\text{D7})$$

with



$$\Lambda_k = \left( \sum_{\alpha,\beta} |c_{\alpha\beta}|^2 \langle \alpha\alpha | R_0 \rangle \langle L_0 | \beta\beta \rangle \right) \left( \sum_{\alpha,\beta} |d_{\alpha\beta}|^2 \langle \alpha\alpha | R_0 \rangle \langle L_0 | \beta\beta \rangle \right), \quad (\text{D8})$$

$$\begin{aligned} \Lambda_k^s = & \left( \sum_{\alpha,\beta} |c_{\alpha\beta}|^2 \langle \alpha\alpha | R_s \rangle \langle L_s | \beta\beta \rangle + \sum_{\alpha \neq \alpha', \beta} c_{\alpha\beta} c_{\alpha'\beta}^* \langle \alpha'\alpha | R_s \rangle \langle L_s | \beta\beta \rangle + \sum_{\alpha, \beta \neq \beta'} c_{\alpha\beta} c_{\alpha\beta'}^* \langle \alpha\alpha | R_s \rangle \langle L_s | \beta'\beta \rangle \right. \\ & \left. + \sum_{\substack{\alpha \neq \alpha', \\ \beta \neq \beta'}} c_{\alpha\beta} c_{\alpha'\beta'}^* \langle \alpha'\alpha | R_s \rangle \langle L_s | \beta'\beta \rangle \right) \left( \sum_{\alpha,\beta} |d_{\alpha\beta}|^2 \langle \alpha\alpha | R_0 \rangle \langle L_0 | \beta\beta \rangle \right). \end{aligned} \quad (\text{D9})$$

Now if we plug  $\lambda_k^N$  in the entropy equation as given in Eq. (38) in the main text, we get

$$\begin{aligned} S(r) &= - \sum_k \Lambda_k \log \Lambda_k - \sum_s \gamma_s^r \left[ \Lambda_k^s + \sum_k \Lambda_k^s \log \Lambda_k \right] - \sum_{ss'} \gamma_s^r \gamma_{s'}^r \frac{\Lambda_k^s \Lambda_k^{s'}}{\Lambda_k}, \\ &= S_0 - \sum_s \gamma_s^r \left[ \sum_k \Lambda_k^s + \sum_k \Lambda_k^s \log \Lambda_k \right] - \sum_{ss'} \gamma_s^r \gamma_{s'}^r \sum_k \frac{\Lambda_k^s \Lambda_k^{s'}}{\Lambda_k}. \end{aligned} \quad (\text{D10})$$

- 
- [1] R. Horodecki, P. Horodecki, M. Horodecki, K. Horodecki, *Quantum entanglement*, Rev. Mod. Phys. **81**, 865 (2009).  
[2] A. Osterloh, L. Amico, G. Falci, R. Fazio, *Scaling of entanglement close to a quantum phase transition*, Nature **416**, 608 (2002).  
[3] T.J. Osborne, M.A. Nielsen, *Entanglement in a simple quantum phase transition*, Phys. Rev. A **66**, 032110 (2002).  
[4] J.M. Maldacena, *The Large N limit of superconformal field theories and supergravity*, Int. J. Theor. Phys. **38**, 1113 (1999).  
[5] S. Ryu, T. Takayanagi, *Holographic derivation of entanglement entropy from AdS/CFT*, Phys. Rev. Lett. **96**, 181602 (2006).  
[6] G. Vidal, *Entanglement Renormalization*, Phys. Rev. Lett. **99**, 220405 (2007).  
[7] M. van Raamsdonk, *Building up spacetime with quantum entanglement*, General Relativity and Gravitation, **42**, 2323 (2010).  
[8] B. Swingle, *Entanglement renormalization and holography*, Phys. Rev. D **86**, 065007 (2012).  
[9] C. Cao, S.M. Carroll, S. Michalakis, *Space from Hilbert Space: Recovering Geometry from Bulk Entanglement*, Phys. Rev. D **95**, 024031 (2017).  
[10] K. Hyatt, J.R. Garrison, B. Bauer, *Extracting entanglement geometry from quantum states*, Phys. Rev. Lett. **119**, 140502 (2017).  
[11] L. Amico, R. Fazio, A. Osterloh, V. Vedral, *Entanglement in many-body systems*, Rev. Mod. Phys. **80**, 517 (2008).  
[12] M. Srenidcki, *Entropy and Area*, Phys. Rev. Lett **71**, 666 (1993).  
[13] J. Eisert, M. Cramer, M.B. Plenio, *Colloquium: Area laws for the entanglement entropy*, Rev. Mod. Phys. **82**, 277 (2010).  
[14] M.M. Wolf, F. Verstraete, M.B. Hastings, J.I. Cirac, *Area Laws in Quantum Systems: Mutual Information and Correlations*, Phys. Rev. Lett. **100**, 070502 (2008).  
[15] C. Holzhey, F. Larsen, and F. Wilczek, *Geometric and Renormalized Entropy in Conformal Field Theory*, Nucl. Phys. B **424**, 443 (1994).  
[16] G. Vidal, J. I. Latorre, E. Rico, A. Kitaev, *Entanglement in Quantum Critical Phenomena*, Phys. Rev. Lett. **90**, 227902 (2003).  
[17] P. Calabrese, J. Cardy. *Entanglement entropy and quantum field theory*. J. Stat. Mech., P06002, 2004.  
[18] P. Calabrese, J. Cardy, *Entanglement entropy and conformal field theory*, J. Phys. A **42**, 504005 (2009).  
[19] G. Vitagliano, A. Riera, and J. I. Latorre, *Volume-law scaling for the entanglement entropy in spin 1/2 chains*, New J. Phys. **12**, 113049 (2010).  
[20] G. Ramírez, J. Rodríguez-Laguna, and G. Sierra, *From conformal to volume-law for the entanglement entropy in exponentially deformed critical spin 1/2 chains*, J. Stat. Mech. P10004 (2014).  
[21] G. Ramírez, J. Rodríguez-Laguna, and G. Sierra, *Entanglement over the rainbow*, J. Stat. Mech. P06002 (2015).  
[22] J. Rodríguez-Laguna, S.N. Santalla, G. Ramírez, G. Sierra, *Entanglement in correlated random spin chains, RNA folding and kinetic roughening*, New J. Phys. **18**, 073025 (2016).  
[23] J. Rodríguez-Laguna, J. Dubail, G. Ramírez, P. Calabrese, and G. Sierra, *More on the rainbow chain: entanglement, space-time geometry and thermal states*, J. Phys. A: Math. Theor. **50**, 164001 (2017).

- [24] E. Tonni, J. Rodríguez-Laguna, and G. Sierra, *Entanglement hamiltonian and entanglement contour in inhomogeneous 1D critical systems*, J. Stat. Mech. 043105 (2018).
- [25] V. Alba, S. N. Santalla, P. Ruggiero, J. Rodríguez-Laguna, P. Calabrese, and G. Sierra, *Unusual area-law violation in random inhomogeneous systems*, J. Stat. Mech. 023105 (2019).
- [26] N. Samos Sáenz de Buruaga, S.N. Santalla, J. Rodríguez-Laguna, and G. Sierra *Symmetry protected phases in inhomogeneous spin chains*, JSTAT 093102 (2019).
- [27] I. MacCormack, A. Liu, M. Nozaki, S. Ryu, *Holographic Duals of Inhomogeneous Systems: The Rainbow Chain and the Sine-Square Deformation Model*, arXiv:1812.10023.
- [28] N. Samos Sáenz de Buruaga, S.N. Santalla, J. Rodríguez-Laguna, G. Sierra, *Piercing the rainbow state: Entanglement on an inhomogeneous spin chain with a defect*, Phys. Rev. B **101**, 205121 (2020).
- [29] S. Singha Roy, S. N. Santalla, J. Rodríguez-Laguna, and G. Sierra, *Entanglement as geometry and flow*, Phys. Rev. B **101**, 195134 (2020).
- [30] Y. Chen, G. Vidal, *Entanglement contour*, J. Stat. Mech. P10011 (2014).
- [31] Q. Wen, *Formulas for partial entanglement entropy*, Phys. Rev. Research **2**, 023170 (2020).
- [32] Q. Wen, *Balanced Partial Entanglement and the Entanglement Wedge Cross Section*, arXiv:2103.00415 [hep-th] (2020).
- [33] D.N. Page, *Average entropy of a subsystem*, Phys. Rev. Lett. **71**, 1291 (1993).
- [34] Y. W. Dai, X. H. Chen, S. Y. Cho, H. Q. Zhou, *Critical exponents of block-block mutual information in one-dimensional infinite lattice systems*, arXiv:2005.07924 (2020).
- [35] F. Verstraete, J. I. Cirac, V. Murg, *Matrix product states, projected entangled pair states, and variational renormalization group methods for quantum spin systems*, Adv. Phys. **57**, 143 (2008).
- [36] J.I. Cirac, F. Verstraete, *Renormalization and tensor product states in spin chains and lattices*, J. Phys. A: Math. Theor. **42**, 504004 (2009).
- [37] R. Orús, *A practical introduction to tensor networks: matrix product states and projected entangled pair states*, Ann. Phys. **349**, 117 (2014).
- [38] M.F. Maghrebi, Z.-X. Gong, A.V. Gorshkov, *Continuous Symmetry Breaking in 1D Long-Range Interacting Quantum Systems*, Phys. Rev. Lett. **119**, 023001 (2017).
- [39] B.S. Shastry, *Exact solution of an  $S = 1/2$  Heisenberg antiferromagnetic chain with long-ranged interactions*, Phys. Rev. Lett. **60**, 639 (1988).
- [40] F.D. Haldane, *Exact Jastrow-Gutzwiller resonating-valence-bond ground state of the spin-1/2 antiferromagnetic Heisenberg chain with  $1/r^2$  exchange*, Phys. Rev. Lett. **60**, 635 (1988).
- [41] I. Frérot, P. Naldesi, T. Roscilde, *Entanglement and fluctuations in the XXZ model with power-law interactions*, Phys. Rev. B **95**, 245111 (2017).
- [42] S. Singha Roy, H.S. Dhar, *Effect of long-range interactions on multipartite entanglement in Heisenberg chains*, Phys. Rev. A **99**, 062318 (2019).
- [43] T. Kennedy, *Exact diagonalisations of open spin-1 chains*, J. Phys.: Condens. Matter **2**, 5737 (1990).
- [44] M. Hagiwara, K. Katsumata, Ian Affleck, B.I. Halperin, J.P. Renard, *Observation of  $S = 1/2$  degrees of freedom in an  $S = 1$  linear-chain Heisenberg antiferromagnet*, Phys. Rev. Lett. **65**, 3181 (1990).
- [45] M.V. Rakov, M. Weyrauch, *Bilinear-biquadratic spin-1 rings: an  $SU(2)$ -symmetric MPS algorithm for periodic boundary conditions*, J. Phys. Commun. **1**, 015007 (2017).
- [46] F.D.M. Haldane, *Nonlinear Field Theory of Large-Spin Heisenberg Antiferromagnets: Semiclassically Quantized Solitons of the One-Dimensional Easy-Axis Néel State* Phys. Rev. Lett. **50**, 1153 (1983).